Single-particle Raman Spectroscopy for studying physical and chemical processes of atmospheric particles

Zhancong Liang[1], Yangxi Chu[2], Masao Gen[3], Chak K. Chan[1]*

[1] School of Energy and Environment, City University of Hong Kong, Hong Kong, 999077, China.

[2] State Key Laboratory of Environmental Criteria and Risk Assessment, Chinese Research Academy of Environmental Sciences, Beijing, 100012, China.

[3] Faculty of Frontier Engineering, Institute of Science and Engineering, Kanazawa University, Kanazawa, 920-1192, Japan.

Correspondence to: Chak K. Chan (chak.k.chan@cityu.edu.hk)

Abstract. Atmospheric particles experience various physical and chemical processes and change their properties during their lifetime. Most studies on atmospheric particles, both in laboratory and field measurements, rely on analyzing an ensemble of particles. Because of different mixing states of individual particles, only average properties can be obtained from studies using emsembles of particles. To better understand the fate and environmental impacts of atmospheric particles, investigations on their properties and processes at a single-particle level are valuable. Among a wealth of analytic techniques, single-particle Raman spectroscopy provides an unambiguous characterization of individual particles under atmospheric pressure in a non-destructive and in-situ manner. This paper comprehensively reviews the application of such a technique in the studies of atmospheric particles, including particle hygroscopicity, phase transition and separation, and solute-water interactions, particle pH, and multiphase reactions. Investigations on enhanced Raman spectroscopy and bioaerosols on a single-particle basis are also reviewed. For each application, we describe the principle and representative examples of studies. Finally, we present our views on future directions on both technique development and further applications of single-particle Raman spectroscopy in studying atmospheric particles.

1 Background

Atmospheric particles or aerosols have considerable effects on climate and human health (Seinfeld and Pandis, 2016). In general, atmospheric particles can originate from a wide variety of anthropogenic and natural sources. Primary particles are emitted directly as a liquid or solid (e.g., soot particles, mineral dust), and they can also undergo atmospheric multiphase reactions. Secondary particles can also be generated by gas-to-particle conversions, such as new particle formation via nucleation and condensation (Pöschl, 2005). During their atmospheric lifetime, both primary and secondary particles are subject to physical and chemical processes, such as partitioning and multiphase reactions. For liquid particles, gas-particle partitioning takes place to achieve thermodynamic equilibrium. For example, an increase or decrease in relative humidity (RH) would result in the uptake of the water vapor into deliquescent particles or the evaporation of particulate water to the gas phase, respectively. Multiphase reactions can be described as gas-particle partitioning accompanied by chemical reactions. Furthermore, photochemistry is an important group of multiphase reactions during the daytime. Both partitioning and chemical reactions can change the composition of the particles, altering their properties such as hygroscopicity, cloud condensation nuclei (CCN) activities, phase state, morphology, reactivity, toxicity, and finally, environmental impacts.

Physical and chemical processes of atmospheric particles have been examined by numerous experimental approaches: a flowing stream of aerosol particles in an open system (flow tube) (Li et al., 2015;Duporté et al., 2017;Heine et al., 2018;Liu and Abbatt, 2020;Liu et al., 2020a;Peng and Jimenez, 2020), a chamber of suspending particles (smog chamber) (Akimoto et al., 1979;Behnke et al., 1988;Liu et al., 2016;Ye et al., 2018;Charan et al., 2019;Liu and Abbatt, 2021;Qin et al., 2021), a collection of deposited particles (Bao et al., 2018;Zhang et al., 2020b), and single particles (Lee and Chan, 2007a;Krieger et al., 2012;Davies and Wilson, 2016;Gen et al., 2019b;Gong et al., 2019;Sullivan et al., 2020). An aerosol flow tube is one of the most common approaches employing a flowing stream of aerosol particles. It enables real-time characterization of reaction products and particulate size under controlled conditions (e.g., RH, temperature), with instruments connected to the exit or different outlets along the flow tube reactor. Oxidation flow reactors (OFR) are analogous to the general aerosol flow tube, but photooxidants (e.g., OH radical) are introduced to examine secondary organic matter formation (Kang et al., 2007;Smith et al., 2009;George and Abbatt, 2010;Keller and Burtscher, 2012). Typically, higher concentrations of

reactive precursor gases than ambient concentrations are used in these flow systems to compensate for the relatively short residential time (e.g., seconds) of the reactants. However, such equivalency of exposure may not necessarily hold (Lee and Chan, 2007b;Chu et al., 2019). Smog chambers enable simulations of various environmental conditions, including gas concentrations, for studying the formation and chemical transformation of particles. The residence time of particles can be extended to a few hours, but other limitations exist, such as long response time to control/change conditions, high cost, and wall loss of particles (Kang et al., 2007). Deposited particles can be studied using a sample-loaded substrate/filter placed in a flowing-gas reactor or a flow tube with its internal wall coated with particles. Environmental conditions can be easily varied, and the reaction time can be very long. An in-situ analyzer for spectroscopic analysis can be equipped (e.g., Raman, Fourier Transform Infrared Spectrometry (FT-IR)) since the particles are immobilized on a substrate/filter. However, using a large number of particles or large particles is usually required to achieve sensitive detection. The influence of particle loading on the reactions and chemical characterization is a challenging question. In general, these approaches produce statistical results of a collection of particles. They may not truly reflect the interaction between gas and particle since the composition of the individual particles may not be identical (Ault and Axson, 2017).

Single-particle characterization has the advantage that the physical and chemical processes undertaken by the particle can be unambiguously monitored. While there is a wealth of instruments for comprehensively characterizing single particles, some are destructive (e.g., mass spectroscopy) or operate under vacuum conditions (e.g., electron microscopy), making them unsuitable for monitoring the gas-particle interaction on the same particles. Single-particle spectroscopic methods (e.g., Raman) can be good alternatives, but the particles are usually supermicron and up to tens of microns. The findings from particles much larger than ambient ones need to be interpreted carefully for drawing implications in submicron atmospheric particles.

Despite its requirements of relatively large particles for spectroscopic signals, single-particle Raman spectroscopy offers several advantages for studying the atmospheric processing of aerosol particles. First of all, a single particle can be unambiguously characterized *in situ* without destruction. From the Raman spectra, chemical compositions of typical aerosol particles (e.g., soot, sulfate, organics, etc.) can be

92 identified by their characteristic peaks. Interactions between molecules can be inferred by peak shifts

93 and changes in peak width. Particulate properties such as the phase state and size can also be

94 characterized by coupling levitation (or isolation) technique and optical microscopy. We will elaborate

95 on the applications of these functions later.

96

97 Furthermore, Raman analysis is operated under atmospheric pressure and enables the use of atmospheric

98 relevant concentrations for a long exposure time to examine atmospheric gas-particle interactions (Lee

99 and Chan, 2007a). Micro-Raman systems provide the spatial information of chemical species at 2-D or

100 even 3-D levels (Batonneau et al., 2006;Sobanska et al., 2006;Tripathi et al., 2009;Scolaro et al.,

101 2009;Sobanska et al., 2014;Offroy et al., 2015;Sobanska et al., 2015;Falgayrac et al., 2018;Ao et al.,

102 2020). Recent advances in stimulated Raman scattering by micro-Raman further improves the spatial

103 resolution from 1 μm to 350 nm and significantly shortens the scanning time from 2.5 h to 2 s (Ao et al.,

104 2020). The disadvantage of Raman spectroscopy is that it can only detect Raman-active functional groups

105 but cannot provide information on the exact molecular structures. Light-absorbing chemicals such as

106 humic-like substances (HULIS) or some brown carbon species may generate fluorescence, interfering

107 with the peak identification in the spectra (Ivleva et al., 2007a). Therefore, single-particle Raman

108 spectroscopy is more suited for laboratory-generated particles than ambient particles. FTIR does not

109 suffer from fluorescence since it uses a longer wavelength (up to tens of μm), but the long wavelength

110 also lowers the spectral resolution (Ault and Axson, 2017;Liu et al., 2020b). Also, Raman has advantages

111 over FTIR for water-containing samples because the strong water peaks in the latter can mask the peaks

112 from other components or even make them undetectable (Nishikida et al., 2018).

113

114 This paper will introduce the general setup of the single-particle Raman spectrometer, how single

115 particles can be characterized unambiguously, and examples of physical and chemical processes reported

116 in the literature. We focus on applications of atmospheric relevance and refer readers to other literature

117 on the principles of Raman spectroscopy and related techniques (e.g., stimulated Raman or coherent

118 Anti-stokes Raman spectroscopy) and applications of less direct atmospheric relevance (Tolles et al.,

119 1977;Efremov et al., 2008;Jones et al., 2019). Finally, we will provide suggestions on future directions

120 of Raman spectroscopy for atmospheric particle studies.

121

2 General set up of single-particle Raman spectroscopy

2.1 Particle isolation

In general, single-particle Raman spectroscopy consists of two key components: particle isolation and Raman spectroscopy, including micro-Raman and confocal Raman configurations. One of the most popular approaches for single-particle isolation is particle levitation, which has been discussed in a few reviews (Reid and Mitchem, 2006;Mitchem and Reid, 2008;Krieger et al., 2012). In this paper, we will briefly introduce their principles and configurations and focus on atmospheric applications. Techniques for levitation of particles can be mainly divided into electrical, optical, and acoustic trapping. Another approach for particle isolation is particle deposition onto substrates with Raman analyses of single particles on an individual basis.

2.1.1 Electrodynamic balance

The Electrodynamic balance (EDB) has been used for studying single particles with a diameter of 1-100μm since the 1980s (Davis and Ray, 1980). A particle is levitated and trapped at the null point under the alternating current (AC) and direct current (DC) electric fields in the EDB. In the absence of other forces, the gravitational force of the particle trapped in the EDB is equal to the balancing electrostatic force, as shown in Eq. (1)

$$mg = nqC\frac{V_{DC}}{z} \tag{1}$$

where m is the mass of the particle, g is the gravitational constant, n is the number of elementary charges present on the particle, q is the elementary charge, z is the distance between two electrodes for the DC voltage, C is a constant dependent on the geometrical configuration of the EDB, and V_{DC} is the balancing DC voltage required to levitate the particle stationary. According to Eq. (1), the mass of the particle is proportional to the DC voltage needed to balance its gravitational force, assuming that the charge present on the trapped particle remains constant. Hence, the relative mass change in the particle undergoing any physical or chemical processing can be quantified by measuring the balancing DC voltage. With a particle levitated stationary, Raman spectroscopy of the stably trapped particles can provide chemical information. Coupled with mass change measurements and optical microscopy, physical and chemical characterization of single particles can be in-situ monitored. In addition to the traditional single-particle EDB (Davis and Ray, 1980;Chan et al., 1992), other EDB set-ups, for

151 example, quadrupole (Q)-EDB and comparative kinetic (CK)-EDB, have been developed. Q-EDB

152 allows the trapping of multiple droplets simultaneously. During chemical reactions, individual

153 particles are released one at a time for mass spectroscopy analysis while the rest of the particles are

154 kept levitated for in-situ spectroscopic characterization (Singh et al., 2017;Jacobs et al., 2017;Singh

155 et al., 2018;Kohli and Davies, 2021). CK-EDB employs a reference droplet with known composition

156 and hygroscopic property, which serves as an accurate probe for the environmental conditions in

157 which the tested droplet is examined. It affords hygroscopicity measurements and mass-transfer

158 kinetic measurements on the droplets at high RH (>99%) (Davies et al., 2013;Rovelli et al.,

159 2016;Marsh et al., 2019).

160

161 **2.1.2 Optical trapping**

162 Optically traps can be basically categories into radiation pressure trap, photophorectic trap and universal

163 optical trap. Radiation pressure trap, which is the most general in studying aerosol particles, utilizes the

164 radiation pressure from a light source to balance the weight of the levitated particle (Ashkin, 1970).

165 During optical trapping, the particle interacts with a highly focused laser beam and experiences scattering

166 and gradient forces (Ashkin and Dziedzic, 1981;Mitchem and Reid, 2008). The scattering force is

167 proportional to the square of the induced dipoles and the intensity of the incident laser beam, acting as a

168 force along the direction of the beam propagation. In contrast, the gradient force derives from the

169 focusing of the laser beam and draws the particle towards the region with the highest light intensity

170 (Krieger et al., 2012).

171

172 Radiation pressure-based optical levitation and optical tweezer are two typical optical-trapping

173 techniques utilizing these two forces. While optical levitation relies on the exact balance between

174 downward gravitational force and upward scattering force, optical tweezers effectively create a strong

175 intensity gradient in three dimensions by tightening the focus of the laser beam to generate amplified

176 gradient forces. Optical tweezers provide a more robust trap with the gradient force typically many orders

177 of magnitude larger than the scattering and gravitational forces, leading to 3-dimensional confinement in

178 position with a single laser beam. However, particle size changes must be accompanied by dynamic

179 changes in the light intensity for retaining the trapped particle. In principle, transparent non-absorbing

180 particles of 1–100 μm in diameter can be trapped with dynamic light intensity adjustment for droplet size

181 changes. By configuring a Bessel laser beam, instead of the typical Gaussian beam, in either vertically

182 or horizontally trapping arrangements, optical levitation and tweezer can be applied for trapping

183 submicron particles (Meresman et al., 2009;Cotterell et al., 2014;Lu et al., 2014). However, Raman

184 spectroscopy would require larger particles for sufficient signal-to-noise ratios. A recent study reported

185 a photochemical study of aerosol particles using an optical trap for the first time by employing a custom-

186 built photochemical levitation chamber (Gómez Castaño et al., 2019). A sidewall of the chamber is

187 equipped with quartz windows for a UV lamp.

188

189 In addition to radiation pressure traps, photophoretic traps and universal optical traps are two emerging

190 alternatives (Redding et al., 2015a;Redding and Pan, 2015). The former is specifically for light-absorbing

191 particles. The latter employs a hollow beam to trap either transparent and light-absorbing particles using

192 radiation pressure force and photophoretic force, respectively (Gong et al., 2018a). Using these

193 techniques, Raman characterizations have been made on light-absorbing particles in recent years,

194 including bioaerosols (Wang et al., 2015a;Redding et al., 2015a;Redding et al., 2015b;Gong et al., 2018b,

195 2019), aromatic compounds (Kalume et al., 2017b;Kalume et al., 2017a;Gong et al., 2018b), carbon

196 nano-tubes (Pan et al., 2012;Gong et al., 2018b) and soot (Uraoka et al., 2017).

197

198 **2.1.3 Acoustic levitation**

199 Compared to the EDB and optical trap, acoustic levitation is less utilized in atmospheric research due to

200 the complicated acoustic streaming and the requirement for large particles (20 μm- 2 mm.) (Cohen et al.,

201 2020;Jones et al., 2021). In an acoustic levitator, high-frequency sound waves generated by a piezo-

202 electric radiator reflect from a concave-shaped reflector to generate a standing wave. The latter produces

203 acoustic radiation pressure on the particle, levitating and trapping it against the gravitational force. It has

204 been reported that a single particle can be firmly trapped by acoustic levitation under 15 h continuous

205 irradiation (Tobon et al., 2017;Seng et al., 2018).

206

207 **2.1.4 Deposited particles**

208 In addition to single-particle levitation, deposited particles on a surface provide a convenient platform

209 for single-particle Raman spectroscopy. While levitation can trap few particles for investigation, surface-

210 based isolation affords a relatively large number of single particles, which can support further off-line

7

211 characterizations. However, the direct contact between particle and substrate may induce solute

212 nucleation or phase separation that causes unexpected modification in particulate morphology. Hence,

213 hydrophobic substrates are often used to study supersaturated aqueous droplets by reducing the particle

214 and substrate contact area. Investigations on photochemistry can be easily performed by coupling a

215 transparent substrate and an additional light source beneath the quartz window at a flow cell's bottom

216 (Gen et al., 2019b;Gen et al., 2020). A single particle can be retained for an infinite time deposited,

217 facilitating studies of slow processes in the atmosphere. However, Raman scattering from the substrate

218 could also show interference.

219

220 **2.2 Raman spectroscopy**

221 A single particle Raman spectroscopy set-up generally involves a laser for excitation, followed by

222 collection optics to detect the Raman signals analyzed by a spectrometer with a monochromator and a

223 CCD detector. The Raman peak location and intensity/area provide information on the speciation and

224 abundance of specific particulate components. Appendix A summarizes the Raman peak assignment of

225 representative atmospheric species. Raman peak can also shift its location (in wavenumber) and change

226 in the full width at half-maxima (FWHM) as a response to variations of local bonding environments,

227 such as molecular interaction and phase transition. Furthermore, Raman emissions from spherical

228 particles (e.g., levitated droplets) can be complicated by resonance modes at discrete wavelengths

229 triggered by cavity-enhanced Raman scattering (CERS) (Miles et al., 2012), or so-called size parameters

230 in the spectra. These resonant modes are often called morphology-dependent resonance (MDRs) or

231 whispering gallery modes (WGMs) (Chan et al., 1991;Krieger et al., 2012). They can accurately

232 determine size with a resolution down to ~5 nm, refractive index, and even shell-core morphology of the

233 mixed organic-inorganic particles based on the Mie theory (Gorkowski et al., 2017;Rafferty and Preston,

234 2018;Sullivan et al., 2020;Gorkowski et al., 2020). The optical effects complicate the Raman

235 measurements for chemical analysis, although they provide additional information for the sizing and

236 refractive index of the particles based on Mie theory. We refer readers to the references for the

237 interactions between Mie scattering and Raman spectroscopy (Chan et al., 1991;Krieger et al.,

238 2012;Nadler et al., 2019). Micro-Raman is a combined system that uses an optical microscope for guiding

239 the laser to analyte particles and collect Raman scattering from the same microscope connected to a

240 spectrometer. The Raman scattering signal-to-noise ratio can be enhanced since the incident laser energy

is focused on a small volume through a high magnification (and short working distance) objective. Furthermore, 2D Raman imaging is possible in studying particles in the order of tens of microns (Eom et al., 2016;Zhao et al., 2018). Confocal Raman micro-spectroscopy eliminates the Raman scattering from volumes other than the focal volume by configuring additional slits in the spectrometer. Confocal Raman provides depth profiles of constituent information of the particle (Scolaro et al., 2009).

This paper focuses on the use of single-particle Raman spectroscopy to examine the physical and chemical processes of atmospheric particles. We describe techniques of particle maneuvering that allow single-particle Raman spectroscopy such as EDB, deposited particles, and optical trapping. However, it is not our intention to conduct a detailed examination of the application of these techniques beyond single-particle Raman spectroscopy. Hence, in this review, we put less emphasis on literature related to other applications of these trapping techniques. We focus on investigating these physical and chemical processes of particles by Raman instead of the particle properties or detailed descriptions of these processes investigated by other techniques. The overall aim of the paper is to introduce single-particle Raman spectroscopy as a useful tool to examine a host of processes of atmospheric relevance.

3 Characterization of single particles

3.1 Hygroscopicity and phase transition

Depending on the environmental RH, type of solutes, and size of the particles (Kelvin effect), atmospheric particles can absorb/release an appropriate amount of water to reach equilibrium with the gas phase, i.e., the partial water vapor pressure above the particle surface equals to that of the gas phase. Hygroscopic properties include water uptake/evaporation and phase transition as a response to changes in ambient RH. Upon water uptake/evaporation, the particle size change alters the particulate capacity in scattering light, and particles can also be activated to cloud condensation nuclei (Tang et al., 2019). In this paper, we focus on subsaturated (RH <100%) environments. The phase states determine the water uptake behaviors of the atmospheric particles (Pajunoja et al., 2016;Rosati et al., 2020). They can be generally divided into liquid (i.e., aqueous), crystalline, and amorphous (e.g., ultra-viscous, gel, rubber, glasses). Both crystalline and amorphous particles are solids, but only the latter can absorb water reversibly, while the former shows hysteresis in water uptake. At increasing RH, water uptake increases the aerosol liquid water (ALW) content of deliquescent/amorphous particles and their size and ability to

271   scatter light. A recent study showed that the poor visibility during haze in the North China Plain is

272   positively correlated to the ALW(Wu et al., 2018b). When crystalline particles are exposed to increasing

273   RH, they will initially adsorb a small amount of water on its surface, the so-called surface adsorbed water

274   (SAW), and then uptake a significant amount of water vapor abruptly to become aqueous droplets at the

275   deliquescence RH (DRH). The DRH is the RH at which a droplet attains the saturated salt concentration,

276   ignoring the influence of the Kelvin effect, which is often the case for single-particle Raman analysis

277   (particle size > 10 μm). At decreasing RH, a droplet loses water to become supersaturated and finally

278   may effloresce to form crystalline particles at the efflorescence RH (ERH). Typical inorganic

279   atmospheric components of $(NH_4)_2SO_4$, NH_4NO_3 and NaCl deliquesce at ~80%, ~62% and ~75% RH

280   but effloresce at 34-48%, 0-30% and 39-54%, respectively. Many studies show that nitrates and some

281   organics do not effloresce even at low RH (e.g., below 5%) (Mikhailov et al., 2009;Yeung and Chan,

282   2010). In general, organics with high solubility (e.g., malonic acid) tend to remain a supersaturated liquid

283   state or amorphous state at low RH (Krieger et al., 2012). Unlike DRH, which is thermodynamically well

284   defined, ERH is a stochastic property that relates to the kinetics of nucleation and presence of impurities.

285   It has been reported that sucrose crystals deliquesce at 85.6%RH upon humidification, but the aqueous

286   droplets turn into a glassy amorphous state upon drying instead of forming crystallized solids (Zobrist et

287   al., 2011). Using EDB and optical trap experiments, hygroscopic changes and phase transition RH values

288   that involve rapid changes in mass or size can be measured by the balancing voltage and light scattering,

289   respectively. The growth factor (GF) in terms of mass or size ratios as a function of water activity or RH,

290   DRH, and ERH can be easily determined by changes in mass/size and the light scattering pattern (Chan

291   et al., 2005;Mitchem et al., 2006;Marsh et al., 2017).

292

293   While GF, DRH, and ERH measurements are readily made for mixed particles using EDB and optical

294   traps, the formation of mixed-phase particles before full deliquescence is more complicated. For example,

295   unlike the corresponding single inorganic salts, NaCl-malonic acid and $(NH_4)_2SO_4$-malonic acid mixed

296   particles absorb a significant amount of water before their DRH since malonic acid absorbs water

297   reversibly without crystallization (Lee et al., 2008a). However, this stepwise water uptake and phase

298   transition behaviors could not be explained by EDB/optical levitation due to the lack of chemical

299   characterization. Raman spectroscopy offers complementary information on the water uptake behaviors

300   and phase states of Raman active species (Yeung and Chan, 2010;Li et al., 2017). For example, the water-

301   to- solute ratio (WSR) as a function of ambient RH can be easily determined from the integrated peak

302   area ratio of the water v(O–H) to that of the solute (e.g., sulfate, nitrate) after proper calibration. Also,

303   the full width at half maxima (FWHM) of the characteristic peaks is sensitive to the phase state of the

304   solute. In general, a species in the liquid phase has a larger FWHM than in the solid phase because the

305   less compact molecular arrangement allows minor variations in vibration. In Fig. 1a,b, as the RH

306   decreased to 39.5% for ammonium sulfate (AS) and 19% for ammonium nitrate (AN), crystallization

307   can be inferred by the red-shift and decrease in FWHM of sulfate and nitrate peaks, and the disappearance

308   of water peak. On this basis, the mixed-phase particle prior to full deliquescence can be characterized by

309   FWHM of different Raman-active components. For instance, Ling and Chan found an increased FWHM

310   of nitrate peak (~730 cm^{-1}) at ~67% RH, followed by an increased FWHM of sulfate peak (~450 cm^{-1})

311   at ~76 RH% for mixed-phase AS-AN particles when RH increased (Fig. 1c,d). These changes indicate

312   that AN deliquesced before AS did upon humidification, and the mixed-phase AS-AN particle was

313   composed mainly of aqueous AN and crystalline AS. The accuracy of single-particle Raman

314   spectroscopy in determining hygroscopicity has been verified by thermodynamic models such as E-AIM

315   and UNIFAC (Peng et al., 2001;Yeung and Chan, 2010). There are numerous hygroscopicity applications

316   on various specific systems, including model inorganics, organics, and their mixtures (Chu et al.,

317   2015;Laskina et al., 2015;Wang et al., 2021b;Tobon et al., 2021;Zhang et al., 2021a;Ashraf et al., 2021)

318   mineral dust (Liu et al., 2008), secondary organic aerosols (Wu et al., 2020), atmospheric-relevant

319   biological macromolecules (Mael et al., 2021) using single particle Raman spectroscopy. It should be

320   noted that evaporation of some components and precipitation of some salts could occur during the

321   RH cycling in hygroscopicity measurements (Li et al., 2017;Cai and Zhao, 2018;Ma et al., 2019a;Ma

322   et al., 2019b;Wu et al., 2020;Li et al., 2021). Single-particle Raman spectroscopy can probe such

323   processes in-situ by the disappearance of some characteristic peaks (evaporation) or changes of their

324   FWHH (precipitation) (Braban et al., 2003;Wang et al., 2017).

325

326   **3.2 Solid-phase transition**

327   In addition to liquid-solid phase changes, transitions can occur between solid phases, from a metastable

328   one to a stable one at a specific temperature. Many organics are known to form polymorphs, defined as

329   solids with the same chemical composition but distinctive properties such as thermal stability and

330   solubility due to different structures (Krieger et al., 2012). Different polymorphs of the same compound

331 can exhibit different Raman characteristics, which can identify different solid states and their transition.

332 For example, crystalline glutaric acid (GA) particles could exist as the metastable α-form and the

333 thermodynamically stable β-form at room temperature, and α-form GA tends to transfer into β-form.

334 Using EDB-Raman, Chan et al. (2006) coated GA on AS particles by coagulation of small GA particles

335 formed by nucleation. Raman spectra showed the existence of α-form GA in the freshly coated particles,

336 but then β-form was detected after a deliquescence - crystallization cycle (Chan et al., 2006). Ling and

337 Chan (2008) reported the formation of the α-form GA solid in a freshly crystallized GA-AS particle.

338 The α-form GA solid gradually transformed to the β-form at 60% RH in 3 h at room temperature (Ling

339 and Chan, 2008). Furthermore, Yeung et al. (2010) examined the effects of polymorphism on the

340 hygroscopic properties of GA particles using Micro-Raman (Yeung et al., 2010). By evaporation at room

341 temperature, α-form and β-form solid particles were formed (α:$\beta \approx 5$:1). It was observed that the α-

342 form deliquesced at 85-86% RH, whereas the β-form deliquesced at 90% RH. Furthermore, the α-form

343 is transformed to the β-form at 86% RH instead of achieving full deliquescence (Fig. 2). This solid

344 phase transition behavior was used to explain the discrepancies of DRH values of glutaric acid particles

345 reported based on different literature measurements (Cruz and Pandis, 2000;Peng et al., 2001;Choi and

346 Chan, 2002;Parsons et al., 2004;Zardini et al., 2008;Treuel et al., 2009). Polymorphism also exists in

347 atmospheric relevant inorganics. For example, AN can exist in five stable polymorphic forms with

348 distinct Raman spectra, depending on the temperature. In atmospheric research, very little attention has

349 been paid to the solid phase transitions of AN because phase IV AN particle is stable over a wide range

350 of tropospheric temperatures ($-17°C \sim 32°C$) (Wu et al., 2007). Nevertheless, Wu and Chan (2008)

351 reported that the KNO_3/AN mixed particles undergo the IV-III transition under ambient temperatures at

352 a relatively high mass percentage of KNO_3($\geq$7.4 wt%), or even crystallize directly in phase III from

353 droplets with a further increase in the mass percentage of KNO_3 (Wu and Chan, 2008).

354

355 Another typical solid phase transition is between stable/metastable double salts. Like metastable/stable

356 polymorphs, metastable double salts show Raman characteristics different from stable ones, likely due

357 to specific molecular interactions. Ling et al. (2007) observed the double-salt 3AN·AS, not predicted

358 from thermodynamics, in the freshly crystallized mixed single particles of AN and AS using single-

359 particle Raman spectroscopy (Ling and Chan, 2007). The existence of double salts indicates that AN and

360 AS likely crystalized simultaneously. The degree of metastability could depend upon the crystallization

361 processes of the particles. Besides, it takes several hours to more than a day, depending on RH, for a

362 freshly crystallized metastable AS-AN double salt particle to reach its stable form, suggesting a high

363 possibility that metastable solids persist in the atmosphere when the ambient RH is sufficiently low. The

364 AN-AS double salts were recently reported in ambient particles in Beijing (Sun et al., 2019b;Wang et al.,

365 2021a).

366

367 **3.3 Molecular interactions between particulate water and solutes**

368 In general, characterizations on phase transitions relies on the sensitivity of Raman spectroscopy in

369 probing the bonding environment of components in the particles. Raman can also characterize the

370 interactions between the solutes and particulate water, such as hydrogen/ionic bonding. For example, the

371 Raman shift of strongly hydrogen-bonded water ($\sim$3500 cm^{-1}) is generally higher than that of water

372 monomers ($\sim$3300 cm^{-1}) (Zhang and Chan, 2003). At low RH, the elevated concentration of electrolytes

373 leads to more significant disruption of the hydrogen bonding environment of the water molecules,

374 resulting in a shift of OH stretching peak at 3480cm^{-1} to higher frequencies. In contrast, the low-

375 frequency shoulder at 3290 cm^{-1} diminishes. Thus, the shape of water peaks in Raman spectra can reflect

376 the ionic strength of the particle, which is an essential parameter for aerosol chemistry (Mitchem et al.,

377 2006;Mekic et al., 2020). The sensitive shift of water peak has also been used in studying ice nucleation

378 properties such as depositional freezing (Wise et al., 2010;Wise et al., 2012) and immersing freezing

379 (Knopf et al., 2002;Knopf et al., 2003). Specifically, while liquid water peaks are usually located at

380 $\sim$3400cm^{-1} with a shoulder at a lower wavenumber, a sharp peak at $\sim$3150 cm^{-1} with shoulder peaks at

381 $\sim$3200cm^{-1} appears as water is frozen (Schill et al., 2014;Mael et al., 2019). Besides, ionic bonding of

382 inorganic salts (e.g., SO_4^{2-}, NO_3^-) can also be reflected by their Raman characteristics; and many of them

383 have been further supported by theoretical calculations (Yu et al., 2012;Wang et al., 2015b;Zhu et al.,

384 2018). For example, Zhang et al. observed a blue shift of sulfate and nitrate Raman peaks and an increase

385 in FWHM when the molar water to the solute ratio (WSR) in $MgSO_4$ and $Mg(NO_3)_2$ particles decreases

386 to less than six, the number of hydration of Mg^{2+} ions (Zhang and Chan, 2000;Zhang et al., 2004). These

387 observations were attributed to direct contacting ion pairs formed between Mg^{2+} and anions, without

388 water molecules between the ions. Besides, single-particle Raman spectroscopic analysis can reveal the

389 structural heterogeneity of droplets. Raman imaging suggested that the NO_3^- to Mg^{2+} ratio of the contact

390 ion pairs increases but the H_2O to Mg^{2+} ratio decreases as the surface of a highly supersaturated droplet

13

391   is approached (Zhang et al., 2004). Yeung and Chan (2010) reported that though no crystallization was

392   shown by glyoxylic acid particle even at 0% RH, a new C=O peak at ~1820cm^{-1} appeared together with

393   the aqueous C=O peak at 1735 cm^{-1}, possibly indicating the presence of anhydrate (Yeung and Chan,

394   2010).

395

396   **3.4 Liquid-liquid phase separation**

397   As mentioned above, partial crystallization can lead to a separation of solid and liquid mixed phases.

398   Separation of two or even more liquid phases, namely liquid-liquid phase separation (LLPS), is also

399   possible (Song et al., 2012a;Song et al., 2018;Huang et al., 2021;Ma et al., 2021). LLPS can be triggered

400   by the interactions between inorganic, organic solutes and particulate water in mixed particles (You

401   et al., 2012;Renbaum-Wolff et al., 2016). This phenomenon is mainly attributed to the low solubility

402   of some non-polar or weakly polar organics, especially in the presence of inorganic salts, which

403   may further decrease the solubilities of organics as the salting-out effects (Setschenow, 1889).

404

405   Optical microscopy (as a part of a single particle Raman microscope) can directly indicate LLPS by the

406   contrasting colors on appearance, based on the different refractive indices of materials in different phases

407   (You et al., 2012). Single-particle (micro-) Raman spectroscopy can examine LLPS via spatial scanning

408   (micro-Raman), optical imaging (micro-Raman), Raman imaging, and whisper gallery modes (WGMs)

409   with additional chemical information of the different phases (Bertram et al., 2011;Song et al., 2012b).

410   Spatial scanning records distinct micro-Raman spectra at different locations of the particle and

411   reveals LLPS (Bertram et al., 2011;Wu et al., 2018a) such as core-shell structures (e.g., an aqueous

412   core surrounded by a BC-containing organic shell) (Brunamonti et al., 2015). However, Raman

413   spatial scanning requires accurate focusing of the laser onto different targeted phases, which can be

414   difficult when phases are separated into multiple small inclusions (Buajarern et al., 2007b).

415

416   Using spatial scanning and optical imaging, Ma et al. (2021) reported an organic shell-aqueous core

417   LLPS in deposited 1, 2, 6-hexanetriol/ammonium sulfate mixed particles. However, different

418   substrates for deposited particles could affect their LLPS behavior (Ma et al., 2021). Though LLPS

419   of an organic/AS mixed particle has been observed on both hydrophobic (i.e., PTFE) and

420   hydrophilic (i.e., glass) substrates, the former shows an organic shell with an AS inner core while

421   the latter shows an opposite configuration (Zhou et al., 2014b). To eliminate interaction with

422   substrates, Ishizaka et al. (2021) used levitated droplets and found both core-shell and partially

423   engulfed LLPS. The observed configurations of two phases are well consistent with thermodynamic

424   predictions based on interfacial tensions and relative volume ratios of two immiscible phases

425   (Ishizaka et al., 2021).

426

427   Another approach for identifying LLPS is Raman imaging of the whole particle in one single

428   measurement. Typical Raman measurements bin the vertical pixels of a CCD to enhance the signal to

429   noise ratio while the horizontal pixels represent the wave number after chromatic dispersion by a grating.

430   Zhang et al. (2004) used collection optics to obtain an image of a particle in an EDB on the slit of a

431   monochromator. Instead of using vertical binning, the vertical pixels registered the vertical profile of the

432   Raman scattering (e.g., edge to center to edge) of the particle (Zhang et al., 2004). Chu and Chan (2017)

433   reported that the core-shell phase separation in a mixed sucrose-ammonium sulfate particle with a sucrose

434   molar fraction of 50% at <5% RH, but not at 70%RH. As shown in Fig. 3a, b (<5% RH), the accumulated

435   C-H signal on the two sides indicates the presence of an organic-rich coating and an organic-deficient

436   core. In contrast, the even distribution of the C-H signal in Fig. 3c (70% RH) suggests that the particle

437   is likely homogeneous (Chu and Chan, 2017a). Kalume et al. (2018) observed temporally resolved LLPS

438   in a diethyl phthalate and glycerol mixed droplet. Upon evaporation, diethyl phthalate migrated to the

439   surface and formed an outer layer and glycerol was more concentrated in the interior of the droplet

440   (Kalume et al., 2018).

441

442   Additionally, WGMs have also been utilized to infer the occurrence of LLPS and the specific

443   particle morphologies. For example, different resonance structures appear in the Raman spectra

444   when core-shell or engulfed phase separation occur (Buajarern et al., 2007a, b;Kwamena et al.,

445   2010;Song et al., 2013;Marcolli and Krieger, 2020). Sharps peaks generated by WGMs in spectra can

446   be found if the spatial distribution of particulate species is symmetric, such as those in core-shell

447   separated and homogeneously mixed particles though the number, location, and intensity of WGMs

448   peaks are different. In contrast, the engulfed phase-separated particles do not show any WGMs

449   peaks (Sullivan et al., 2020). Utilizing WGMs, Steward et al. (2015) reported the transition between

450   partially-engulfed and core-shell structure at different RH values (Stewart et al., 2015). However,

451   these analyses focus on WGMs but not Raman as a chemical probing technique.

452

453   **3.5 Determination of pH**

454   The pH, defined as the activity of proton in aerosol particles, can also be inferred from Raman spectra

455   based on the intensity of the conjugate acid/base ion pairs. Sulfate/bisulfate has been used most frequently.

456   The pH can be determined by substituting the conjugate ion pair concentrations and its dissociation

457   coefficient into Henderson-Hasselbalch (H-H) (Radić and Prkić, 2012), Debye-Hückel theory, and

458   specific ion interaction theory equations, respectively (Ciavatta, 1980;Rindelaub et al., 2016;Craig et al.,

459   2017;Craig et al., 2018;Coddens et al., 2019;Chang et al., 2020a). The latter two are more suitable to

460   supersaturated particles since non-ideality has been considered. Rindelaub et al. (2016) reported direct

461   measurements of pH in individual deposited particles according to sulfate/bisulfate peaks in Raman

462   spectra, and its variation with RH (Rindelaub et al., 2016). Craig et al. (2017) extended this approach to

463   a range of atmospherically relevant inorganic and organic acid-base equilibria systems covering a wide

464   range of pH (-1~10) (Craig et al., 2017). To eliminate the artifact of contacts between the particle and

465   the substrate, Coddens et al. (2019) determined the pH of trapped particles via titration by coalescence

466   of droplets containing strong acids (Coddens et al., 2019). Boyer et al. (2020) further utilized the WGMs

467   for determining the solute concentration in real-time and achieve uncertainties in pH measurements of

468   picoliter droplets ranging from ±0.03 to 0.06 pH units (Boyer et al., 2020). Very recently, Cui et al. (2021)

469   reported that water can be used to probe pH in individual model aerosol particles (e.g., $(NH_4)_2SO_4$, NaCl),

470   since the water bands are affected by other components (e.g., ions), as discussed in Sec.3.3. Specifically,

471   the broad water peak at 2600-3800 cm^{-1} could comprise many overlapping peaks, representing O-H

472   vibration of water molecules in different local environments. The addition of solutes affects the local

473   environment of water molecules, and changes the relative intensities of the overlapped peaks. Hence, the

474   activity of specific solutes can be obtained by analyzing the overlapped water peaks after rigorous

475   calibration; and the pH of the aerosol particle can be calculated (Cui et al., 2021).

476

477   **4 Multiphase reactions**

478   In Section 3, applications of characterizing single particles have been reviewed. This section mainly

479   focuses on the "processes" occurring on single particles. Taking water-solute interactions as an example,

480   hygroscopicity describes the ability of solutes to absorb water upon equilibrium at fixed RH. Water

481 uptake is a dynamic process, although it is generally too quick to be a limiting step in most atmospheric

482 applications. However, in some viscous matrixes, the water uptake rate could be reduced by orders of

483 magnitude due to the limited diffusion (Chang et al., 2020b). Taking advantage of the different Raman

484 characteristics of D_2O and H_2O, Davies and Wilson (2016) measured the diffusion coefficients of water

485 molecules in trapped viscous particles by monitoring the isotopic exchange rate using Raman

486 spectroscopy (Davies and Wilson, 2016). Determination of kinetic parameters of non-reactive processes

487 such as partitioning coefficient, diffusion coefficient, and mass accommodation coefficient has been

488 reviewed in another paper (Krieger et al., 2012). Hence, applications on probing multiphase reactions

489 using single-particle Raman spectroscopy will be the focus below.

490

491 **4.1 Multiphase formation of secondary inorganic aerosols (SIA)**

492 Particulate sulfate and nitrate are two major secondary inorganic aerosols (SIA). They have dominant

493 Raman peaks at ~980 cm^{-1} and ~1046 cm^{-1}, respectively. Probing multiphase formation of sulfate by

494 single-particle Raman spectroscopy was first employed by Davis and co-workers for absorption of SO_2

495 by alkali-metal hydroxides particles (Aardahl and Davis, 1996). In atmospheric applications, particulate

496 sulfate formation has been a debating topic since the currently proposed pathways, including O_3, OH

497 radical, NO_2, H_2O_2, and transition metal ions (TMI) in cloud water, cannot entirely account for the high

498 concentration of sulfate observed in haze events such as those in the North China Plain (NCP) (Cheng et

499 al., 2016). Using single-particle micro-Raman spectroscopy, Chan and his group reported that oxidants

500 including NO_2, N(III), OH radicals, etc., generated from particulate nitrate photolysis could effectively

501 oxidize SO_2 to sulfate (Gen et al., 2019b;Gen et al., 2019c;Zhang et al., 2020a;Zheng et al., 2020b). Clear

502 increase of the sulfate peak signal was identified in Raman spectra of UV irradiated nitrate particle (Fig.

503 4). Later, they also reported sulfate formation by multiphase oxidation of SO_2 during $FeCl_3$ photolysis

504 (Gen et al., 2020). Angle et al. (2021) reported an enhanced sulfate formation in TMI-containing droplets

505 compared to that in TMI bulk solutions. This enhancement is greater than that can be explained by the

506 higher TMI/bisulfite concentrations in aerosol than in bulk. It suggests that surface effects and potentially

507 aerosol pH gradients play important roles in the S(IV) oxidation process in aqueous aerosols (Angle et

508 al., 2021).

509

510 The formation of nitrate has also been investigated. Zangmeister and Pemberton (2001) performed

kinetic analysis on the reactions between deposited NaCl particles and gaseous HNO_3 based on the increase of the nitrate peak (Zangmeister and Pemberton, 2001). Tang et al. (2014) coupled optical levitation with Raman spectroscopy to investigate N_2O_5 uptake on SiO_2 particle as a function of RH and found that particulate nitrate formation increased as RH increased. They conclude that the water content affects the partitioning of HNO_3 between the gas phase and condensed phases (i.e., adsorbed phase and aqueous phase). More surface adsorbed water layers block the reactive sites for N_2O_5 uptake but promote HNO_3 dissolution (Tang et al., 2014). Scolaro et al. (2009) studied the three-dimensional evolution of the NaCl(100) surface during its reaction with NO_2 as a function of RH, using confocal Raman imaging combined with non-contact atomic force microscopy (AFM) (Scolaro et al., 2009). At 0% RH, a $NaNO_3$ monolayer capping the NaCl(100) surface formed. $NaNO_3$ tetrahedral crystals (<0.5 μm) formed at 45% RH, and supermicron $NaNO_3$ rhombohedral plates were obtained under the H_2O multilayer regime (45%<RH<75%). At RH>80%, both crystalline and aqueous NO_3^- were found. Reactions were accelerated in the presence of water vapor due to the formation of reactive HNO_3 by NO_2 hydrolysis. Ault et al. (2014) reported that individual nascent sea spray aerosol particles showed different reactivity toward HNO_3 and N_2O_5, likely due to compositional heterogeneity. After the same exposure of gaseous reactants, some particles showed intense $v(NO_3^-)$ peak, whereas $v(C-H)$ is still the dominant mode in some other particles (Ault et al., 2014).

There are also investigations on the simultaneous formation of particulate sulfate and nitrate. Zhao et al. (2018) reported a multi-step reaction mechanism of oxidation of SO_2 by NO_2 on deposited $CaCO_3$ particles(Zhao et al., 2018). Further, Yu and Zhao et al. (2018) reported that the uptake coefficient of SO_2 on $CaCO_3$ particles in the presence of O_2/NO_2 mixture was much higher than that without O_2 (Yu et al., 2018). The synergy of NO_2 and O_2, which involved mechanisms such as chain reactions, resulted in much faster sulfate formation than the sum of the reaction rates with NO_2 and with O_2 alone. These reports show the usefulness of single-particle Raman spectroscopy in studying the multiphase formation of particulate sulfate and nitrate. It is worth mentioning that degradation of organo-sulfate has been proposed to produce particulate inorganic sulfate recently (Xu et al., 2020b) and organo-sulfate functional groups are also Raman-active (Bondy et al., 2018). Raman spectroscopy may find applications in the study of organo-sulfates.

4.2 Multiphase formation of SOA

Most of the organic compounds are Raman-active though some of them may not have strong signals. Some generate fluorescence in general orders of magnitude stronger than Raman emissions, masking useful Raman features of particles. The characteristic peaks of a single organic compound are generally more than that of an inorganic one due to its complex molecular vibration modes, and the reaction products may further complicate spectra analysis. Therefore, investigation on the multiphase formation of SOA by Raman spectroscopy is limited. However, though identifying the molecular nature of the products is difficult, single-particle Raman spectroscopy can provide useful information during secondary organic aerosol (SOA) formation. For example, Lee et al. (2008) observed a gradually elevating baseline in Raman spectra during acid-catalyzed octanol uptake by levitated sulfuric acid particles at 10% RH but not at 50% RH (Lee et al., 2008b). Though the speciation of products could not be resolved, the increasing fluorescence is evident, attributable to the formed SOA in the particles. Using an EDB, Chan and Chan (2011) examined the dependence of nonanal on the presence of hydrophilic and hydrophobic organics in acidic mixed organic-sulfuric acid particles. The presence of hydrophobic organic materials (oleic acid and its reaction products with sulfuric acid) enhanced SOA formation by reactive uptake of nonanal, likely through an enhanced dissolution of nonanal in the particles (Chan and Chan, 2011). In contrast, levoglucosan, a hydrophilic organic, did not increase the uptake coefficient of nonanal. It is suggested that acid-catalyzed reactive uptake should be examined with the explicit consideration of the role of particle-phase organics that are either initially present or accumulated as a reaction product. Using micro-Raman, Olson et al. (2019) investigated the uptake of isoprene epoxydiol (IEPOX) by α-pinene SOA/toluene SOA-coated AS particles (Olson et al., 2019). Before the uptake, both coated AS particles show core-shell morphology. $v(N-H)$ and $v(SO_4^{2-})$ were found at ~3200cm^{-1} and ~976cm^{-1} in the particle core, while strong $v(C-H)$ at 2800-3000cm^{-1} and other moderate/weak stretches of C-H were found in the shell region. After the uptake, $v(C-H)$ and $v(RO-SO_3)$ were found in the particle core, indicating SOA formation, such as organo-sulfate. No organo-sulfate was detected in shell regions of both types of particles, although decreases of $v(C-H)$ peak were apparent. Generally, Raman analysis is useful for kinetic analysis of reactions (e.g., measuring uptake coefficients), but it is challenging to reveal complicated mechanisms due to the limited molecular identification. For better examining the reaction mechanism, deposited particles can be extracted for off-line analysis using mass spectrometry (MS) (Li et al., 2008;Chan et al., 2013).

571

572   4.3 Multiphase oxidation of aerosol particles

573   In addition to reactive uptake of SOA precursors, single-particle Raman spectroscopy has also been used

574   to explore the uptake of oxidants by organic aerosol particles. So far, the reported studies are limited to

575   ozonolysis. Raman spectroscopy is well suited in ozonolysis studies because the C=C bonds and the

576   peroxide groups are Raman-active, and ozonolysis does not generate strongly fluorescent products.

577   Using single-particle Raman spectroscopy, Lee and Chan (2007) performed in-situ observations of the

578   particle mass, hygroscopicity, morphology of the oleic acid (Lee and Chan, 2007a), linolenic acid, and

579   linoleic acid particles (Lee and Chan, 2007b) during ozonolysis. They found that low ozone concentration

580   (~200−250 ppb) with a longer exposure period (20 h) favors autoxidation to form C=C−C=C groups;

581   but an extremely high ozone concentration (~10 ppm) at shorter exposure time (2 h) tends to form

582   carboxylic acids (C=O), secondary ozonide (O-O), hydroxyalkyl hydroperoxide (O-H), etc (Enami and

583   Colussi, 2017;Qiu et al., 2020). Chu et al. (2019) further examined the interchangeability between ozone

584   concentration and exposure time by studying ozonolysis of linoleic acid particles in a broader range of

585   experimental conditions. They found the interchangeability holds at ozone exposure $\leq$ 500 ppb h and [O_3]

586     $\leq$ 100 ppb for the formation of autoxidation products containing conjugated diene structures but does not

587   hold for the decay of parent linoleic acid or at higher [O_3] (Chu et al., 2019). These results indicate that

588   extrapolating experimental results of the ozonolysis under high [O_3] conditions to ambient levels should

589   be carried out with caution. Single-particle Raman spectroscopy also enables us to infer the volatilization

590   of some ozonolysis products. For example, Lee and Chan (2007) found that the mass of oleic acid

591   particles was observed to decrease with time while that of linoleic acid and linolenic acid increased on

592   the contrary, which could be potentially explained by the different volatility of the ozonolysis products

593   (Lee and Chan, 2007b). King et al. (2004) reported an optical tweezers study of ozonolysis of oleic acid

594   and synthetic seawater droplets. They found clear Raman signatures indicating nonanoic acid and

595   nonanal production, followed by their gradual disappearance, which is also likely due to the volatilization

596   (King et al., 2004). Furthermore, Dennis-Smither et al. (2012) used optical tweezers to study the

597   oxidation of oleic acid droplets containing an inorganic seed with a time-resolution of 1 s to resolve the

598   reactive loss of ozone and the evaporative loss of products. The oleic acid ozonolysis was completed in

599   ~3000 s, but the decrease of droplet volume still lasts for an additional ~5000 s due to the slow

600   volatilization of the products (Dennis-Smither et al., 2012).

601

Chan and Chan (2012) studied the roles of the phase state and water content in the ozonolysis of maleic acid (MA) and AS mixed particles. Aqueous MA was found to be more reactive toward ozone than crystalline MA. Interestingly, they also found that higher water content favors more efficient ozonolysis, although the concentration of MA is accordingly lower (Chan and Chan, 2012). Furthermore, ozonolysis of optically trapped bioaerosol particles has also been reported. In general, lipids and proteins show distinct v(C-H) peaks at 2855 cm^{-1} and 2928 cm^{-1}, respectively (Kline and Treado, 1997;Rygula et al., 2013;Czamara et al., 2015). The ratio of these peaks can be thus used for inferring the different susceptibilities of lipids and proteins during ozonolysis oxidation (Gong et al., 2019). The products derived from oxidations such as carbonyls (C=O; ~1700 cm^{-1}) (Lee and Chan, 2007b) and oligomer of cysteine (C-S; ~662cm^{-1}) (Movasaghi et al., 2007;Kampf et al., 2015) are also detected.

612

There are also studies exploring other organic surrogates of atmospheric aerosol with more complicated structures. For example, King et al. (2008) measured the uptake coefficients of ozone on fumarate and benzoate droplets (as a proxy of HULIS-containing aerosol) and α-pinene droplets (a proxy of biogenic organic aerosol) (King et al., 2008). Different reaction products such as carbonate were identified in Raman spectra, though the chemical characterization is not comprehensive due to their volatility and the detection limits. The reaction of α-pinene in the droplet phase was more than one order faster than in bulk aqueous solutions, likely due to more effective diffusion of ozone in the gas phase and more efficient mass accommodation at the air-droplet interface (King et al., 2008). Milsom et al. (2021) reported the ozonolysis of fatty acid-soap mixed particles, using oleic acid and sodium oleate as models. In these particles, the strong interactions between the soap carboxylate and the carboxylic acid form crystalline structures (Milsom et al., 2021). Upon ozonolysis, the decay of C=C (~1600cm^{-1}) was faster in liquid oleic acid droplets than crystalline oleic acid-soap particles, although the crystalline structure was eventually broken by ozonolysis. Uraoka et al. (2017) studied the multiphase reactions of optically-trapped soot particles with ozone and OH radicals. C=O vibrations were observed under both ozone and OH exposure. The graphitic domain was suggested to undergo OH oxidation based on the increase in the ratio of the disorder (D) to the graphite (G) domain from Raman spectra (Uraoka et al., 2017).

629

4.4 Amine/Ammonia reactions

Ammonia and amines are the most abundant alkaline gases in the atmosphere. They play a significant role in new particle formation and buffering aerosol pH by neutralization of acidic particles (Kirkby et al., 2011;Almeida et al., 2013;Zhang et al., 2015;Kerminen et al., 2018;Zheng et al., 2020a). There are three types of reactions involving ammonia and amines: (1) Neutralization reaction between acidic particles and ammonia/amines; (2) Displacement of ammonia by amines from ammonium salt particles and vice versa from aminium salt particles; (3) Reactions between ammonia/amines and dissolved di-carbonyls or between gaseous di-carbonyls and ammonium/aminium salt particles, both would result in the formation of colored compounds (i.e., Brown carbon; BrC).

Based on the strong vibration signal of the C-H bond ($\sim$2900cm^{-1}, sharp peak) from amine/aminium salts and the N-H bond ($\sim$2800-3300 cm^{-1}, broad peak), the uptake of amine and ammonia can be easily studied using single-particle Raman spectroscopy. Sauerwein and Chan (2017) explored the role of phase state in simultaneous uptake of ammonia and dimethylamine (DMA) by acidic particles (e.g., sulfuric acid and oxalic acid) (Sauerwein and Chan, 2017). Anhydrous acidic particles were inert and took up DMA and ammonia presumably by adsorption only. The uptake rates of DMA and ammonia by aqueous acidic droplets were found comparable initially, but once the droplets were neutralized, the stronger base DMA displaced some of the particulate ammonium. On the other hand, if crystallization took place during the uptake, DMA uptake was inhibited, but continuous ammonia uptake gradually displaced the particle DMA ions.

Chan and Chan (2013) reported that the exchange reactions of ammonia/amine vapors in aqueous particles were reversible, and the exchange rates of aqueous particles were, in general, higher than those of their corresponding solid counterparts. Compared with crystalline solids (e.g., methylammonium sulfate), amorphous solid (e.g., diethylammonium sulfate) was found with a higher exchange rate, likely due to the less compact molecular structure (Chan and Chan, 2013). Chu and Chan (2017) further examined the effect of a hydrophilic viscous organic surrogate and a hydrophobic organic coating on DMA uptake by AS. Both the viscous materials and the fresh and aged organic coating retarded DMA uptake by mass transfer limitation (Chu and Chan, 2017b, a). The uptake of DMA by crystalized AS particles at 10-30% RH resulted in the deliquescence of the particles, likely due to the presence of surface adsorbed water (SAW) that promoted the dissolution of DMA. Once dimethylaminium sulfate is formed,

661 it absorbs more water since it is more hygroscopic than AS and further promoted DMA uptake (Chu and

662 Chan, 2017a). As crystalline solids are generally considered inert towards reactions, this finding indicates

663 that SAW on crystals can serve as a medium to facilitate gas uptake.

664

665 BrC has attracted increasing attention due to its atmospheric abundance and capacity in regulating

666 radiative balance (Laskin et al., 2015). The reactions between dicarbonyls and ammonium/aminium-

667 containing salt particles can form BrC. Gen et al. (2018) investigated the multiphase uptake of glyoxal

668 by ammonium salt-containing particles using Micro-Raman spectroscopy. They found a gradual

669 elevation of the baseline, which was attributed to the formation of a fluorescent BrC (i.e., 2,2′-

670 biimidazole, BI), based on off-line analysis by UV-VIS spectroscopy and fluorescence spectroscopy

671 (Gen et al., 2018a). The reduction in ALW at low RH increases the glyoxal uptake rate via the enhanced

672 "salting-in" effect and the BI formation rate by facilitating dehydration reactions. Mabato et al. (2019)

673 examined glyoxal uptake by methylaminium salt-containing particle. Although the "salting-in" effect

674 was also found in methylaminium salt-containing particles, enhanced BI formation was not observed,

675 likely due to the higher hygroscopicity of methylaminium salt (i.e., higher ALW content) than ammonium

676 salt (Mabato et al., 2019).

677

678 **4.5 Photochemistry of aerosol particles**

679 A particular type of aerosol particle reaction that deserves special attention is photochemical reactions,

680 which can be initiated by irradiation of the particles. Nitrate can be photolyzed under atmospheric

681 irradiation ($\lambda>290nm$). Nitrate photolysis proceeds via three channels: one produces NO_2 and OH

682 radicals, another produces NO_2^- and $O(^3P)$ and the last generates $ONOO^-$. The third channel's quantum

683 yield is considered negligible compared with the former two since ONOO is unstable. It has been

684 reported that NO_2^- and ONOO- peaks increased, but NO_3^- peaks decreased in the Raman spectra of

685 acoustically levitated nitrate particles irradiated by UV (Tobon et al., 2017). NO_2 does not have a large

686 absorption cross-section, but it may be hydrolyzed into NO_2^- (Tobon et al., 2017;Seng et al., 2018;Gómez

687 Castaño et al., 2019). Most nitrate photolysis products are oxidants, so their ability to initiate oxidation

688 reactions has also been explored (Gen et al., 2019b;Gen et al., 2019c;Zhang et al., 2020a). The production

689 of sulfate via nitrate photolysis was discussed earlier. Recently, Zhang et al. (2021) reported a prominent

690 formate production by glyoxal oxidation during particulate nitrate photolysis, instead of the more

691 commonly found oxalic acids oligomers in the oxidation of glyoxal in bulk solutions (Zhang et al.,

692 2021b). Furthermore, Liang et al. (2021) reported nitrate photolysis in particles containing sucrose,

693 which was used as a surrogate for atmospheric viscous organics. They found that the viscosity of the

694 particle did not reduce the nitrate photolysis rate, but it limited the diffusion of gaseous products (e.g.,

695 NO_x, NO_y) from nitrate photolysis. At a high sucrose fraction and 30%RH, the production of these

696 gaseous products and the particles' viscosity transformed the droplets into "hollow and enlarged" semi-

697 solid particles (Liang et al., 2021).

698

699 Size dependence of nitrate photochemistry has been recently reported, based on single-particle Raman

700 spectroscopy. Tobon et al. studied photolysis acoustically levitated nitrate particles (40~80μm) at 254nm

701 UV radiation. No change in Raman spectra for 2 h. In contrast, smaller particles (5~8μm) trapped

702 optically yielded various Raman peaks of nitrate photolysis products (Tobon et al., 2017;Gómez Castaño

703 et al., 2019). The slow photolysis in the larger nitrate particles was attributed to the self-inhibited surface

704 process. Additionally, an uneven distribution of NO_2^- inside the smaller particle was also observed

705 through Raman mapping (Gómez Castaño et al., 2019). Organics in the aerosol particle may also

706 decompose under light. For example, Parmentier et al. reported photodegradation of optically trapped

707 oleic acid droplets under 532 nm and 660 nm irradiation, likely initiated by photosensitization. However,

708 they cautioned that degradation loss of optically trapped particles might be artifacts (Parmentier et al.,

709 2021). The photo-decay of light-absorbing particulate matters is also of great interest in understanding

710 their fate in the atmosphere. However, there are very limited studies of atmospheric photochemical

711 reactions using Raman spectroscopy, partly because of the need for complementary chemical speciation

712 for detailed mechanistic studies.

713

714 **5 Enhanced Raman spectroscopy**

715 Though Raman has been used to study physical and chemical processes of atmospheric particles, most

716 of the studies used large particles (dozens of microns) and focused on lab-generated particles with a few

717 representative components. That is primarily because of the intrinsic diffraction limitation of Raman

718 measurements that the laser beam cannot be effectively focused to a spot smaller than its wavelength and

719 thus limits the detection of particles to larger than 1 micron or so. Fluorescence can also be a complication

720 in some chemical systems.

721

722   Various methods have been developed to improve the Raman signal-to-noise ratios and the spatial

723   resolution in other research fields such as material science and biology. Surface-enhanced Raman

724   spectroscopy (SERS) and Tip-enhanced Raman spectroscopy (TERS) have been recently employed in

725   atmospheric research. SERS and TERS enhance Raman emissions by the localized surface plasmon

726   resonances using noble metal nanoparticles (NPs) to provide "hot spots" near the contacting sites between

727   the analyte and NPs (Ault and Axson, 2017). According to the SERS electromagnetic (EM) enhancement

728   theory, the relationship between the SERS intensity (I) and the local EM strength (E) follows $I \propto |E|^4$.

729   The relationship between E and the distance between NPs and analytes (D) is described as $E \propto (1/D)$

730   (Zhou et al., 2015). Hence, maximizing E and minimizing D without inducing significant perturbation

731   to the sample is the primary goal. In addition to this physical enhancement based on the electromagnetic

732   field, Raman signals can also be enhanced chemically. Specifically, molecular/ionic species can attach

733   to the surface of NPs, distorting the molecular structure and increasing the absorption cross-section.

734   Consequently, the Raman signal of an adsorbed species can be enhanced, potentially accompanied by a

735   peak shift (Craig et al., 2015;Gen and Chan, 2017).

736

737   SERS enables the measurements of single particles smaller than 1 micron. Craig et al. (2015) found that

738   the signals from individual submicron (down to 0.6 μm) particles could be effectively detected with

739   intensity enhancement (Craig et al., 2015). Furthermore, Tirella et al. (2018) extended the SERS

740   detection to the accumulation mode (800~150 nm) particles (Tirella et al., 2018). Sun et al. (2019)

741   reported a size-resolved (covering both coarse mode and accumulation mode) SERS characterization

742   study of atmospheric particles sampled during haze events (Sun et al., 2019a;Sun et al., 2019b). More

743   recently, Kunihisa et al. (2020) reported sensitive SERS measurement of Aiken mode particles (<100nm)

744   by combining a condensational growth tube sampler (CGT) and a SERS substrate for directly sampling

745   (Kunihisa et al., 2020). The wide analytical range of particle size enables SERS to be a potentially

746   powerful tool in studying ambient particulate matters (Steer et al., 2016;Vejpongsa et al., 2017;Chen et

747   al., 2021).

748

749   Some species including components of microorganisms (Tahir et al., 2020), microplastics (Xu et al.,

750   2020a), crystalline silica (Zheng et al., 2018), the fine structure of organics (Craig et al., 2015;Fu et al.,

751 2017;Gen et al., 2018b), and even some Raman-active inorganic salts at very low concentration (Saniel

752 et al., 2019) are invisible in normal Raman due to their weak Raman-activities. However, they could be

753 detected with a SERS substrate. The sensitive detection by SERS can provide valuable insight into

754 particle transformations and emission sources (Vejpongsa et al., 2017;Ghosal and Wall, 2019;Lee et al.,

755 2019). However, the enhancement factor of SERS is not constant. It strongly depends on the distribution

756 and quantity of noble metal NPs and the hotspots over the substrate, making quantitative analysis difficult.

757 Many attempts have been made to explore preferable and tunable substrate for generalizable atmospheric

758 particle detection (Xu et al., 2020a;Cheng et al., 2021), but still more progresses are needed in the future.

759

760 The most common SERS application uses particles deposited on SERS substrates, relying on the "hot

761 spot" locating beneath the analyte particles. Recently, some studies create innovative interactions

762 between particulate analytes and SERS NPs to enhance SERS detections. Wei et al. (2018) used 4-

763 mercaptobenzoic acid-functionalized AuNPs as pH nanoprobes and internal SERS substrate and found

764 the existence of a stable pH gradient inside aqueous particles (Wei et al., 2018). Hence, the assumption

765 of homogeneous mixing might not always be correct, and pH predictions by thermodynamic model might

766 underestimate the acidity of interfacial layers of particles, which is crucial for multiphase uptake or

767 surface reactions. As a further investigation of the SERS pH nanoprobe, Huang et al. (2020) reported

768 that the pH distribution inside aerosol particles is affected by the internal distribution of ions, which may

769 depend on the ionic speciation. While sodium tends to reside in the bulk of the particle, leading to a high

770 centroid pH, ammonium distributes more evenly due to its increased surface propensity (Huang et al.,

771 2020).

772

773 Gen et al. developed an electrospray system (ES-SERS) to deposit SERS NPs onto the surface of the

774 analyte particle and found that this technique can selectively enhance the peak intensity of the species

775 located at surface layers such as surface adsorbed water (Gen and Chan, 2017) and organic coatings (Gen

776 et al., 2019a). In a typical micro-Raman set-up, the objective is above the analyte particle. When the

777 analyte particle is deposited on the SERS substrate, the SERS hot spots are located beneath the particle.

778 In other words, upon laser irradiation from the top, the photons generated by excitation need to pass

779 through the particle with a refractive index greater than air, which would scatter or absorb light and thus

780 reduces the signals received by the Raman microscope. In contrast, ES-SERS hot spots are created on

781 the surface of the particle using electrospray. This configuration reduces the loss of photons and affords

782 greater enhancement in the Raman intensity. (Fig. 5) Besides, as the SERS effect is much more prominent

783 near the hot spots (i.e., small D), the location of the hot spots determines where will be probed in SERS

784 spectra. Therefore, while typical SERS substrate collects enhanced Raman signals from the substrate-

785 particle interface, the ES-SERS can provide information from the gas-particle interface, where many

786 atmospheric multiphase processes occur. Sivaprakasam et al. reported real-time SERS measurements of

787 electrostatically trapped particles containing analyte molecules and NPs as internally mixed liquid

788 particles or coating on solid particles (Sivaprakasam et al., 2017;Sivaprakasam and Hart, 2021). The

789 interaction between NPs and analyte increased due to more contact areas than that between an aerosol

790 particle and a substrate.

791

792 Similarly, TERS can produce enhanced Raman signals even from particles in the nucleation mode. TERS

793 is a combination of atomic force microscope (AFM) and Raman spectrometer. In general, AFM

794 determines the topography of a single deposited particle by detecting the interaction force between the

795 AFM tip and the surface of the analytes. In a typical TERS set-up, the AFM tip is coated with noble

796 metal particles. An enhanced Raman signal is generated when the tip is interacting with analytes under

797 laser excitation (Rodriguez et al., 2015). The lack of chemical information of AFM is complemented by

798 SERS. Thus, TERS enables simultaneous characterization of particulate topography and surface species

799 of submicron particles at a high spatial resolution (Ofner et al., 2016). TERS also has the potential for

800 quantitative analysis since the quantity and configuration of hotspots on the tip are constant.

801

802 **6 Bioaerosols**

803 Bioaerosols have attracted increasing attention worldwide dramatically due to the COVID-19 epidemic.

804 Studies using normal Raman/SERS for off-line detection of biological samples (Félix-Rivera and

805 Hernández-Rivera, 2012;Mosier-Boss, 2017), real-time sensing of bioaerosol (Huffman et al., 2020)

806 have been reviewed in detail elsewhere. Bioaerosols have various Raman active components such as

807 phosphate lipid (δ (=C-H), ~1268cm^{-1}; v(C-H), ~2855cm^{-1}), protein (amides bands, ~1260cm^{-1},

808 ~1600cm^{-1}, ~1660cm^{-1}; C-C backbone stretching in β-sheet proteins, ~983cm^{-1}; v(C-H), ~2928cm^{-1}) and

809 nucleic acids (e.g., adenine, ~735cm^{-1}), etc (Socrates, 2004;Rygula et al., 2013;Talari et al., 2015).

810 However, Raman signals from bioaerosol particles are generally weak. To amplify the signals, bioaerosol

811 particles are trapped or deposited onto a substrate for longer integration time (Laucks et al.,

812 2000;Sengupta et al., 2005;Tripathi et al., 2009;Wang et al., 2015a;Redding et al., 2015b;Ai et al., 2020).

813 Using a higher energy laser can also enhance Raman intensity, but it may cause damage to bioaerosol

814 (e.g., fragmentation) (Gong et al., 2017). On this basis, SERS is more suitable than normal Raman

815 spectroscopy. SERS can also quench the fluorescence generated by biomolecules such as tryptophan and

816 tyrosine (Gong et al., 2017).

817

818 In general, there are two strategies of single-particle SERS of bioaerosols: (1) directly sampling

819 bioaerosols on a SERS substrate; (2) moving mixed colloids of SERS NPs and bioaerosols onto a glass

820 substrate, followed by drying. While the former is more convenient without complex pretreatments

821 (Tahir et al., 2020), the latter enables flexible modification of NPs properties. For example,

822 functionalized surface of NPs with tag molecules (e.g., antibody), so-called label-based SERS (Liu et al.,

823 2010), were used for detecting specific biomaterials with high reproducibility. Label-free SERS refers to

824 that without tag molecules, such as Au@Ag. In general, by simply mixing, NPs distribute on biomaterials

825 without specific interactions, and the SERS reproducibility is limited. However, by coating AgNPs on

826 the cell wall of bacteria (Zhou et al., 2014a;Zhou et al., 2015), SERS enhancement was ~30-folds

827 reproducibly higher than simply mixed colloid−bacterial suspension. Furthermore, the discrimination of

828 live and dead bacteria was possible. NPs can be directly formed inside some specific bacteria via bio-

829 reduction for probing the intercellular structure (Jarvis et al., 2008). Overall, SERS can be an innovative

830 tool in bioaerosol characterization, but the antibacterial effect of NPs and heat effect due to excitation

831 laser should be considered (Mosier-Boss, 2017). More examples of bioaerosol detection can be found in

832 a recent review (Liu et al., 2017).

833

834 **7 Future directions**

835 This review paper has shown examples of single-particle Raman spectroscopy in studying atmospheric

836 processes. Overall, the water content, phase state, morphology, and chemical composition of single

837 particles during physical and chemical processes at controlled RH can be monitored in situ.

838 Hygroscopicity and phase behaviors covering a wide range of RH after these processes can also be

839 comprehensively assessed by performing evaporation-humidification cycle measurements (Chan et al.,

840 2006;Chan and Chan, 2007;Liu et al., 2008;Chen et al., 2020). Although fluorescence may exist in some

841   particles, it could be potentially reduced or even eliminated by (1) using longer excitation wavelengths

842   (e.g., 785 and 1064 nm); (2) employing SERS/TERS; (3) photo-bleaching of fluorescent substances

843   under UV-VIS illumination.(Gong et al., 2017) There are many other innovative studies built on trapping,

844   manipulating, and observing multi-particles via Raman (Mitchem and Reid, 2008;Davies, 2019), such as

845   measuring viscosity and diffusion coefficient (Power et al., 2013;Nakajima et al., 2021), probing reaction

846   (Aardahl, 1998;Rkiouak et al., 2014) and phase transition (Richards et al., 2020). Based on these

847   functions and research progresses, we would like to provide the following suggestions on future

848   directions:

849

850   ● **Hyphenated single-particle Raman spectroscopy.** Raman spectroscopy is non-destructive, so

851   incorporating other spectroscopic techniques for characterizing the same particle is possible.

852   Vibrational sum frequency generation spectroscopy (SFG), Fourier transform infrared spectroscopy

853   (FT-IR), and fluorescence spectroscopy, which are also non-destructive, could be complementary

854   to Raman in probing chemical composition of single particle. Recently, novel combination of EDB

855   and mass spectrometry was reported, which can directly introduce the trapped particle for mass

856   spectrometry analysis (Jacobs et al., 2017;Birdsall et al., 2018;Willis et al., 2020). Adaption of this

857   technique with Raman to form an EDB – Raman system with subsequent MS analysis is relatively

858   straight forward. For optical properties, UV/Vis spectroscopy could be a promising choice (Jones

859   et al., 2021). While general laser-based MDR can easily bleach light-absorbing molecules, a recent

860   study reported that MDR modes under broad band excitation can measure refractive index (RI) of

861   light-sensitive samples (Price et al., 2020). Such MDR measuremens can complement in-situ

862   Raman spectroscopy for chemical characterization. Additionally, SERS/TERS are emerging useful

863   approaches, but current SERS/TERS methods for atmospheric research mainly use bare NPs. The

864   direct contact of NPs to analyte molecules can potentially induce chemical enhancement, which

865   could complicate the identification of the phase transition and functional groups (Craig et al.,

866   2015;Gen and Chan, 2017). To remove the chemical enhancement, future studies on chemically

867   inert NPs such as shell-isolated nanoparticle-enhanced Raman spectroscopy (SHINERS) are

868   suggested (Li et al., 2010;Anema et al., 2011).

869

870   ● **Multiphase reaction studies based on single-particle Raman spectroscopy.** Single-particle

871   Raman spectroscopy enables investigations of various atmospheric reactions, including those in

872   surface adsorbed water for solids, mixed-phase particles (solid, aqueous, organic), supersaturated

873   droplets, atmospheric aging of bioaerosols and ultrafast reactions. For solid particles (e.g.,

874   crystalline, mineral dust), multiphase reactions can be "mediated" by surface adsorbed water layers

875   and may result in phase transition, turning the particle into liquid for further reactions (Kuwata and

876   Martin, 2012;Chu and Chan, 2017a;Zhao et al., 2018;Yu et al., 2018;Gen et al., 2019a). Probing

877   heterogenous reactions on the particle surface is possible via ES-SERS, TERS, and normal Raman

878   imaging. As particle constituents can be unevenly distributed (e.g., in LLPS) within a single particle,

879   chemistry may not be the same between the bulk and the surface layers (Wei et al., 2018;Olson et

880   al., 2019;Qiu et al., 2019;Huang et al., 2020;Lam et al., 2021). The studies of the atmospheric

881   processing of pre-existing particles to form secondary aerosols can be further extended to the aging

882   of bioaerosols (Gong et al., 2019). Using pulse laser for excitation, time-resolved resonance Raman

883   spectroscopy (TR3) can be a promising tool in probing short-lived reactive intermediates (e.g.,

884   triplet state molecules). In particular, it helps deepen our understanding in ultrafast reactions or

885   initiation steps of typical reactions (Sahoo et al., 2011;Collins et al., 2018).

886

887 •   **Particle size and temperature effects.** Many publications report single-particle Raman

888   spectroscopy studies under different environmental conditions, including RH and gas concentration,

889   etc. However, how experimental conditions such as temperature and particle size affect kinetics and

890   products in multiphase reactions remains ambiguous. For example, various pathways and kinetic

891   parameters have been proposed to explain particulate sulfate formation in winter haze events in

892   northern China (Chan and Yao, 2008;Su et al., 2020;Liu et al., 2021). However, most studies are

893   based on experimental results at room temperature or 298K. Further exploration with respect to the

894   effect of low temperature on the properties of the particles and multiphase sulfate chemistry is still

895   warranted. Employing a temperature-controlled cold plate flow cell - Raman system for deposited

896   single particles (Wheeler et al., 2015;Mael et al., 2019;Roy et al., 2020), investigations of

897   temperature-dependent reaction kinetics can be easily achieved. Temperature control in a small

898   levitation chamber is also more convenient than in a flow tube or smog chamber. To date, almost

899   all single-particle Raman studies involve supermicron particles. While equilibrium measurements

900   are not sensitive to size (assuming the Kelvin effect is considered), kinetic analysis is often size-

901   dependent. Hence, uptake coefficients for multiphase reactions are usually reported and are

902   restricted to experimental conditions that gas and liquid phase transport are not the rate-limiting

903   step. The size detection limit of single-particle Raman spectroscopy can be extended to sub-10

904   micrometer with high sensitiveity using high-energy excitation laser and tighter optical focusing.

905   The effect of temperature and particle size on multiphase chemistry should be further investigated

906   using long integration time, novel optical configuration (e.g., confocal micro-Raman), and

907   SERS/TERS, etc. Although it is challenging to study single submicron particles by Raman

908   spectroscopy regularly, Raman characterization of a collection of single submicron particles is

909   feasible.

910

917

918 **Reference**

919 Aardahl, C. L., and Davis, E. J. P. B.: Gas/Aerosol Chemical Reactions in the NaOH-SO2-H2O System,
920   Applied Spectroscopy, 50, 71-77, 1996.

921 Aardahl, C. L. W. J. F. D. E. J.: Raman Analysis of Chemical Reactions Resulting from the Collision of
922   Micrometer-Sized Particles, Applied Spectroscopy, 52, 47-53, 1998.

923 Ai, Y., Alali, H., Pan, Y.-L., Videen, G., and Wang, C.: Single-particle optical-trapping raman
924   spectroscopy for the detection and identification of aerosolized airborne biological particles,
925   Measurement Science and Technology, 10.1088/1361-6501/abd5f1, 2020.

926 Akimoto, H., Hoshino, M., Inoue, G., Sakamaki, F., Washida, N., and Okuda, M.: Design and
927   characterization of the evacuable and bakable photochemical smog chamber, Environmental
928   Science & Technology, 13, 471-475, 1979.

929 Almeida, J., Schobesberger, S., Kürten, A., Ortega, I. K., Kupiainen-Määttä, O., Praplan, A. P., Adamov,
930   A., Amorim, A., Bianchi, F., and Breitenlechner, M.: Molecular understanding of sulphuric
931   acid–amine particle nucleation in the atmosphere, Nature, 502, 359-363, 2013.

932 Anema, J. R., Li, J.-F., Yang, Z.-L., Ren, B., and Tian, Z.-Q.: Shell-Isolated Nanoparticle-Enhanced
933   Raman Spectroscopy: Expanding the Versatility of Surface-Enhanced Raman Scattering,
934   Annual Review of Analytical Chemistry, 4, 129-150, 10.1146/annurev.anchem.111808.073632,
935   2011.

Angle, K. J., Neal, E. E., and Grassian, V. H.: Enhanced Rates of Transition-Metal-Ion-Catalyzed Oxidation of S(IV) in Aqueous Aerosols: Insights into Sulfate Aerosol Formation in the Atmosphere, Environmental Science & Technology, 55, 10291-10299, 10.1021/acs.est.1c01932, 2021.

Ao, J., Feng, Y., Wu, S., Wang, T., Ling, J., Zhang, L., and Ji, M.: Rapid, 3D Chemical Profiling of Individual Atmospheric Aerosols with Stimulated Raman Scattering Microscopy, Small Methods, 4, 1900600, https://doi.org/10.1002/smtd.201900600, 2020.

Ashkin, A.: Acceleration and Trapping of Particles by Radiation Pressure, Physical Review Letters, 24, 156-159, 10.1103/PhysRevLett.24.156, 1970.

Ashkin, A., and Dziedzic, J.: Observation of optical resonances of dielectric spheres by light scattering, Appl. Opt., 20, 1803-1814, 1981.

Ashraf, H., Guo, Y., Wang, N., Pang, S., and Zhang, Y.-H.: Hygroscopicity of Hofmeister Salts and Glycine Aerosols–Salt Specific Interactions, The Journal of Physical Chemistry A, 125, 1589-1597, 2021.

Ault, A. P., Guasco, T. L., Baltrusaitis, J., Ryder, O. S., Trueblood, J. V., Collins, D. B., Ruppel, M. J., Cuadra-Rodriguez, L. A., Prather, K. A., and Grassian, V. H.: Heterogeneous Reactivity of Nitric Acid with Nascent Sea Spray Aerosol: Large Differences Observed between and within Individual Particles, The Journal of Physical Chemistry Letters, 5, 2493-2500, 10.1021/jz5008802, 2014.

Ault, A. P., and Axson, J. L.: Atmospheric Aerosol Chemistry: Spectroscopic and Microscopic Advances, Analytical Chemistry, 89, 430-452, 10.1021/acs.analchem.6b04670, 2017.

Bao, F., Li, M., Zhang, Y., Chen, C., and Zhao, J.: Photochemical Aging of Beijing Urban PM2.5: HONO Production, Environmental Science & Technology, 52, 6309-6316, 10.1021/acs.est.8b00538, 2018.

Batonneau, Y., Sobanska, S., Laureyns, J., and Bremard, C.: Confocal Microprobe Raman Imaging of Urban Tropospheric Aerosol Particles, Environmental Science & Technology, 40, 1300-1306, 10.1021/es051294x, 2006.

Behnke, W., Holländer, W., Koch, W., Nolting, F., and Zetzsch, C.: A smog chamber for studies of the photochemical degradation of chemicals in the presence of aerosols, Atmospheric Environment (1967), 22, 1113-1120, 1988.

Bertram, A., Martin, S., Hanna, S., Smith, M., Bodsworth, A., Chen, Q., Kuwata, M., Liu, A., You, Y., and Zorn, S.: Predicting the relative humidities of liquid-liquid phase separation, efflorescence, and deliquescence of mixed particles of ammonium sulfate, organic material, and water using the organic-to-sulfate mass ratio of the particle and the oxygen-to-carbon elemental ratio of the organic component, Atmospheric Chemistry & Physics, 11, 2011.

Birdsall, A. W., Krieger, U. K., and Keutsch, F. N.: Electrodynamic balance–mass spectrometry of single particles as a new platform for atmospheric chemistry research, Atmospheric Measurement Techniques, 11, 33-47, 2018.

Bondy, A. L., Craig, R. L., Zhang, Z., Gold, A., Surratt, J. D., and Ault, A. P.: Isoprene-Derived Organosulfates: Vibrational Mode Analysis by Raman Spectroscopy, Acidity-Dependent Spectral Modes, and Observation in Individual Atmospheric Particles, The Journal of Physical Chemistry A, 122, 303-315, 10.1021/acs.jpca.7b10587, 2018.

Boyer, H. C., Gorkowski, K., and Sullivan, R. C.: In Situ pH Measurements of Individual Levitated Microdroplets Using Aerosol Optical Tweezers, Analytical Chemistry, 92, 1089-1096,

980   10.1021/acs.analchem.9b04152, 2020.

981   Braban, C. F., Carroll, M. F., Styler, S. A., and Abbatt, J. P.: Phase transitions of malonic and oxalic acid
982   aerosols, The Journal of Physical Chemistry A, 107, 6594-6602, 2003.

983   Brunamonti, S., Krieger, U. K., Marcolli, C., and Peter, T.: Redistribution of black carbon in aerosol
984   particles undergoing liquid-liquid phase separation, Geophysical Research Letters, 42, 2532-
985   2539, 2015.

986   Buajarern, J., Mitchem, L., and Reid, J. P.: Characterizing Multiphase Organic/Inorganic/Aqueous
987   Aerosol Droplets, The Journal of Physical Chemistry A, 111, 9054-9061, 10.1021/jp074366a,
988   2007a.

989   Buajarern, J., Mitchem, L., and Reid, J. P.: Characterizing the Formation of Organic Layers on the
990   Surface of Inorganic/Aqueous Aerosols by Raman Spectroscopy, The Journal of Physical
991   Chemistry A, 111, 11852-11859, 10.1021/jp075021v, 2007b.

992   Cai, C., and Zhao, C.: Optical levitation measurement on hygroscopic behaviour and SVOC vapour
993   pressure of single organic/inorganic aqueous aerosol, Atmospheric Environment, 189, 50-60,
994   https://doi.org/10.1016/j.atmosenv.2018.06.040, 2018.

995   Carey, D. M., and Korenowski, G. M.: Measurement of the Raman spectrum of liquid water, The Journal
996   of chemical physics, 108, 2669-2675, 1998.

997   Chan, C. K., Flagan, R. C., and Seinfeld, J. H.: Resonance structures in elastic and Raman scattering
998   from microspheres, Appl. Opt., 30, 459-467, 10.1364/AO.30.000459, 1991.

999   Chan, C. K., Flagan, R. C., and Seinfeld, J. H.: Water activities of NH4NO3/(NH4)2SO4 solutions,
1000   Atmospheric Environment. Part A. General Topics, 26, 1661-1673,
1001   https://doi.org/10.1016/0960-1686(92)90065-S, 1992.

1002   Chan, C. K., and Yao, X.: Air pollution in mega cities in China, Atmospheric Environment, 42, 1-42,
1003   10.1016/j.atmosenv.2007.09.003, 2008.

1004   Chan, K. M., Huang, D. D., Li, Y. J., Chan, M. N., Seinfeld, J. H., and Chan, C. K.: Oligomeric products
1005   and formation mechanisms from acid-catalyzed reactions of methyl vinyl ketone on acidic
1006   sulfate particles, Journal of Atmospheric Chemistry, 70, 1-18, 2013.

1007   Chan, L. P., and Chan, C. K.: Enhanced Reactive Uptake of Nonanal by Acidic Aerosols in the Presence
1008   of Particle-Phase Organics, Aerosol Science and Technology, 45, 872-883,
1009   10.1080/02786826.2011.567314, 2011.

1010   Chan, L. P., and Chan, C. K.: Roles of the Phase State and Water Content in Ozonolysis of Internal
1011   Mixtures of Maleic Acid and Ammonium Sulfate Particles, Aerosol Science and Technology,
1012   46, 781-793, 10.1080/02786826.2012.665514, 2012.

1013   Chan, L. P., and Chan, C. K.: Role of the aerosol phase state in ammonia/amines exchange reactions,
1014   Environmental science & technology, 47, 5755-5762, 2013.

1015   Chan, M. N., Choi, M. Y., Ng, N. L., and Chan, C. K.: Hygroscopicity of Water-Soluble Organic
1016   Compounds in Atmospheric Aerosols: Amino Acids and Biomass Burning Derived Organic
1017   Species, Environmental Science & Technology, 39, 1555-1562, 10.1021/es049584l, 2005.

1018   Chan, M. N., Lee, A. K., and Chan, C. K.: Responses of ammonium sulfate particles coated with glutaric
1019   acid to cyclic changes in relative humidity: Hygroscopicity and Raman characterization,
1020   Environmental science & technology, 40, 6983-6989, 2006.

1021   Chan, M. N., and Chan, C. K.: Mass transfer effects on the hygroscopic growth of ammonium sulfate
1022   particles with a water-insoluble coating, Atmospheric Environment, 41, 4423-4433,
1023   https://doi.org/10.1016/j.atmosenv.2007.01.047, 2007.

Chang, P., Chen, Z., Zhang, Y., and Liu, Y.: Direct measurement of aerosol pH in individual malonic acid and citric acid droplets under different relative humidity conditions via Raman spectroscopy, Chemosphere, 241, 124960, 2020a.

Chang, P., Gao, X., Cai, C., Ma, J., and Zhang, Y.: Effect of waiting time on the water transport kinetics of magnesium sulfate aerosol at gel-forming relative humidity using optical tweezers, Spectrochimica Acta Part A: Molecular and Biomolecular Spectroscopy, 228, 117727, https://doi.org/10.1016/j.saa.2019.117727, 2020b.

Charan, S. M., Huang, Y., and Seinfeld, J. H.: Computational Simulation of Secondary Organic Aerosol Formation in Laboratory Chambers, Chemical Reviews, 119, 11912-11944, 10.1021/acs.chemrev.9b00358, 2019.

Chen, H., Duan, F., Du, J., Yin, R., Zhu, L., Dong, J., He, K., Sun, Z., and Wang, S.: Surface-enhanced Raman scattering for mixing state characterization of individual fine particles during a haze episode in Beijing, China, Journal of Environmental Sciences, 104, 216-224, https://doi.org/10.1016/j.jes.2020.12.008, 2021.

Chen, X., Chu, Y., Lee, A. K., Gen, M., Kasthuriarachchi, N. Y., Chan, C. K., and Li, Y. J.: Relative humidity history affects hygroscopicity of mixed particles of glyoxal and reduced nitrogenous species, Environmental science & technology, 54, 7097-7106, 2020.

Cheng, H., Dong, X., Yang, Y., Feng, Y., Wang, T., Tahir, M. A., Zhang, L., and Fu, H.: Au nanoring arrays as surface enhanced Raman spectroscopy substrate for chemical component study of individual atmospheric aerosol particle, Journal of Environmental Sciences, 100, 11-17, https://doi.org/10.1016/j.jes.2020.07.003, 2021.

Cheng, Y., Zheng, G., Wei, C., Mu, Q., Zheng, B., Wang, Z., Gao, M., Zhang, Q., He, K., Carmichael, G., Pöschl, U., and Su, H.: Reactive nitrogen chemistry in aerosol water as a source of sulfate during haze events in China, Science Advances, 2, e1601530, 10.1126/sciadv.1601530, 2016.

Choi, M. Y., and Chan, C. K.: The Effects of Organic Species on the Hygroscopic Behaviors of Inorganic Aerosols, Environmental Science & Technology, 36, 2422-2428, 10.1021/es0113293, 2002.

Chu, Y., Sauerwein, M., and Chan, C. K.: Hygroscopic and phase transition properties of alkyl aminium sulfates at low relative humidities, Physical Chemistry Chemical Physics, 17, 19789-19796, 2015.

Chu, Y., and Chan, C. K.: Reactive Uptake of Dimethylamine by Ammonium Sulfate and Ammonium Sulfate–Sucrose Mixed Particles, The Journal of Physical Chemistry A, 121, 206-215, 10.1021/acs.jpca.6b10692, 2017a.

Chu, Y., and Chan, C. K.: Role of oleic acid coating in the heterogeneous uptake of dimethylamine by ammonium sulfate particles, Aerosol Science and Technology, 51, 988-997, 10.1080/02786826.2017.1323072, 2017b.

Chu, Y., Cheng, T. F., Gen, M., Chan, C. K., Lee, A. K. Y., and Chan, M. N.: Effect of Ozone Concentration and Relative Humidity on the Heterogeneous Oxidation of Linoleic Acid Particles by Ozone: An Insight into the Interchangeability of Ozone Concentration and Time, ACS Earth and Space Chemistry, 3, 779-788, 10.1021/acsearthspacechem.9b00002, 2019.

Ciavatta, L.: The specific interaction theory in evaluating ionic equilibria, Ann. Chim.(Rome), 70, 551, 1980.

Coddens, E. M., Angle, K. J., and Grassian, V. H.: Titration of Aerosol pH through Droplet Coalescence, J Phys Chem Lett, 10, 4476-4483, 10.1021/acs.jpclett.9b00757, 2019.

Cohen, L., Quant, M. I., and Donaldson, D. J.: Real-Time Measurements of pH Changes in Single,

Acoustically Levitated Droplets Due to Atmospheric Multiphase Chemistry, ACS Earth and Space Chemistry, 4, 854-861, 10.1021/acsearthspacechem.0c00041, 2020.

Collins, D. B., Hems, R. F., Zhou, S., Wang, C., Grignon, E., Alavy, M., Siegel, J. A., and Abbatt, J. P. D.: Evidence for Gas-Surface Equilibrium Control of Indoor Nitrous Acid, Environ Sci Technol, 52, 12419-12427, 10.1021/acs.est.8b04512, 2018.

Cotterell, M. I., Mason, B. J., Carruthers, A. E., Walker, J. S., Orr-Ewing, A. J., and Reid, J. P.: Measurements of the evaporation and hygroscopic response of single fine-mode aerosol particles using a Bessel beam optical trap, Physical Chemistry Chemical Physics, 16, 2118-2128, 2014.

Craig, R. L., Bondy, A. L., and Ault, A. P.: Surface Enhanced Raman Spectroscopy Enables Observations of Previously Undetectable Secondary Organic Aerosol Components at the Individual Particle Level, Analytical Chemistry, 87, 7510-7514, 10.1021/acs.analchem.5b01507, 2015.

Craig, R. L., Nandy, L., Axson, J. L., Dutcher, C. S., and Ault, A. P.: Spectroscopic Determination of Aerosol pH from Acid–Base Equilibria in Inorganic, Organic, and Mixed Systems, The Journal of Physical Chemistry A, 121, 5690-5699, 10.1021/acs.jpca.7b05261, 2017.

Craig, R. L., Peterson, P. K., Nandy, L., Lei, Z., Hossain, M. A., Camarena, S., Dodson, R. A., Cook, R. D., Dutcher, C. S., and Ault, A. P.: Direct Determination of Aerosol pH: Size-Resolved Measurements of Submicrometer and Supermicrometer Aqueous Particles, Analytical Chemistry, 90, 11232-11239, 10.1021/acs.analchem.8b00586, 2018.

Cruz, C. N., and Pandis, S. N.: Deliquescence and Hygroscopic Growth of Mixed Inorganic−Organic Atmospheric Aerosol, Environmental Science & Technology, 34, 4313-4319, 10.1021/es9907109, 2000.

Cui, X., Tang, M., Wang, M., and Zhu, T.: Water as a probe for pH measurement in individual particles using micro-Raman spectroscopy, Analytica Chimica Acta, 1186, 339089, https://doi.org/10.1016/j.aca.2021.339089, 2021.

Czamara, K., Majzner, K., Pacia, M. Z., Kochan, K., Kaczor, A., and Baranska, M.: Raman spectroscopy of lipids: a review, Journal of Raman Spectroscopy, 46, 4-20, 2015.

Davies, J. F., Haddrell, A. E., Rickards, A. M. J., and Reid, J. P.: Simultaneous Analysis of the Equilibrium Hygroscopicity and Water Transport Kinetics of Liquid Aerosol, Analytical Chemistry, 85, 5819-5826, 10.1021/ac4005502, 2013.

Davies, J. F., and Wilson, K. R.: Raman Spectroscopy of Isotopic Water Diffusion in Ultraviscous, Glassy, and Gel States in Aerosol by Use of Optical Tweezers, Analytical Chemistry, 88, 2361-2366, 10.1021/acs.analchem.5b04315, 2016.

Davies, J. F.: Mass, charge, and radius of droplets in a linear quadrupole electrodynamic balance, Aerosol Science and Technology, 53, 309-320, 10.1080/02786826.2018.1559921, 2019.

Davis, E. J., and Ray, A.: Single aerosol particle size and mass measurements using an electrodynamic balance, Journal of Colloid and Interface Science, 75, 566-576, 1980.

Dennis-Smither, B. J., Hanford, K. L., Kwamena, N.-O. A., Miles, R. E. H., and Reid, J. P.: Phase, Morphology, and Hygroscopicity of Mixed Oleic Acid/Sodium Chloride/Water Aerosol Particles before and after Ozonolysis, The Journal of Physical Chemistry A, 116, 6159-6168, 10.1021/jp211429f, 2012.

Duporté, G., Riva, M., Parshintsev, J., Heikkinen, E., Barreira, L. M. F., Myllys, N., Heikkinen, L., Hartonen, K., Kulmala, M., Ehn, M., and Riekkola, M.-L.: Chemical Characterization of Gas- and Particle-Phase Products from the Ozonolysis of α-Pinene in the Presence of Dimethylamine,

Environmental Science & Technology, 51, 5602-5610, 10.1021/acs.est.6b06231, 2017.

Efremov, E. V., Ariese, F., and Gooijer, C.: Achievements in resonance Raman spectroscopy: Review of a technique with a distinct analytical chemistry potential, Analytica chimica acta, 606, 119-134, 2008.

Enami, S., and Colussi, A. J.: Criegee Chemistry on Aqueous Organic Surfaces, The Journal of Physical Chemistry Letters, 8, 1615-1623, 10.1021/acs.jpclett.7b00434, 2017.

Eom, H.-J., Gupta, D., Cho, H.-R., Hwang, H. J., Hur, S. D., Gim, Y., and Ro, C.-U.: Single-particle investigation of summertime and wintertime Antarctic sea spray aerosols using low-Z particle EPMA, Raman microspectrometry, and ATR-FTIR imaging techniques, Atmospheric Chemistry and Physics, 16, 13823-13836, 2016.

Falgayrac, G., Siepka, D., Stefaniak, E. A., Penel, G., and Sobanska, S.: Influence of collecting substrate on the Raman imaging of micron-sized particles, Analytica Chimica Acta, 1014, 41-49, https://doi.org/10.1016/j.aca.2018.02.015, 2018.

Félix-Rivera, H., and Hernández-Rivera, S. P.: Raman Spectroscopy Techniques for the Detection of Biological Samples in Suspensions and as Aerosol Particles: A Review, Sensing and Imaging: An International Journal, 13, 1-25, 10.1007/s11220-011-0067-0, 2012.

Fu, Y., Kuppe, C., Valev, V. K., Fu, H., Zhang, L., and Chen, J.: Surface-Enhanced Raman Spectroscopy: A Facile and Rapid Method for the Chemical Component Study of Individual Atmospheric Aerosol, Environmental Science & Technology, 51, 6260-6267, 10.1021/acs.est.6b05910, 2017.

Gen, M., and Chan, C. K.: Electrospray surface-enhanced Raman spectroscopy (ES-SERS) for probing surface chemical compositions of atmospherically relevant particles, Atmospheric Chemistry & Physics, 17, 2017.

Gen, M., Huang, D. D., and Chan, C. K.: Reactive Uptake of Glyoxal by Ammonium-Containing Salt Particles as a Function of Relative Humidity, Environ Sci Technol, 52, 6903-6911, 10.1021/acs.est.8b00606, 2018a.

Gen, M., Huang, D. D., and Chan, C. K.: Reactive uptake of glyoxal by ammonium-containing salt particles as a function of relative humidity, Environmental science & technology, 52, 6903-6911, 2018b.

Gen, M., Kunihisa, R., Matsuki, A., and Chan, C. K.: Electrospray surface-enhanced Raman spectroscopy (ES-SERS) for studying organic coatings of atmospheric aerosol particles, Aerosol Science and Technology, 53, 760-770, 10.1080/02786826.2019.1597964, 2019a.

Gen, M., Zhang, R., Huang, D. D., Li, Y., and Chan, C. K.: Heterogeneous SO2 Oxidation in Sulfate Formation by Photolysis of Particulate Nitrate, Environmental Science & Technology Letters, 6, 86-91, 10.1021/acs.estlett.8b00681, 2019b.

Gen, M., Zhang, R., Huang, D. D., Li, Y., and Chan, C. K.: Heterogeneous Oxidation of SO2 in Sulfate Production during Nitrate Photolysis at 300 nm: Effect of pH, Relative Humidity, Irradiation Intensity, and the Presence of Organic Compounds, Environ Sci Technol, 53, 8757-8766, 10.1021/acs.est.9b01623, 2019c.

Gen, M., Zhang, R., Li, Y., and Chan, C. K.: Multiphase Photochemistry of Iron-Chloride Containing Particles as a Source of Aqueous Chlorine Radicals and Its Effect on Sulfate Production, Environmental Science & Technology, 54, 9862-9871, 10.1021/acs.est.0c01540, 2020.

George, I. J., and Abbatt, J. P.: Heterogeneous oxidation of atmospheric aerosol particles by gas-phase radicals, Nat Chem, 2, 713-722, 10.1038/nchem.806, 2010.

Ghosal, S., and Wall, S.: Identifying regional soil as the potential source of PM2.5 particulate matter on

air filters collected in Imperial Valley, California – A Raman micro-spectroscopy study, Environmental Pollution, 253, 181-189, https://doi.org/10.1016/j.envpol.2019.07.004, 2019.

Gómez Castaño, J. A., Boussekey, L., Verwaerde, J. P., Moreau, M., and Tobón, Y. A.: Enhancing Double-Beam Laser Tweezers Raman Spectroscopy (LTRS) for the Photochemical Study of Individual Airborne Microdroplets, Molecules, 24, 3325, 2019.

Gong, Z., Pan, Y.-L., Videen, G., and Wang, C.: The temporal evolution process from fluorescence bleaching to clean Raman spectra of single solid particles optically trapped in air, Chemical Physics Letters, 689, 100-104, https://doi.org/10.1016/j.cplett.2017.09.064, 2017.

Gong, Z., Pan, Y.-L., Videen, G., and Wang, C.: Optical trapping and manipulation of single particles in air: Principles, technical details, and applications, Journal of Quantitative Spectroscopy and Radiative Transfer, 214, 94-119, https://doi.org/10.1016/j.jqsrt.2018.04.027, 2018a.

Gong, Z., Pan, Y.-L., Videen, G., and Wang, C.: Optical trapping-Raman spectroscopy (OT-RS) with embedded microscopy imaging for concurrent characterization and monitoring of physical and chemical properties of single particles, Analytica Chimica Acta, 1020, 86-94, 2018b.

Gong, Z., Pan, Y.-L., Videen, G., and Wang, C.: Chemical reactions of single optically trapped bioaerosols in a controlled environment, Aerosol Science and Technology, 53, 853-859, 10.1080/02786826.2019.1621984, 2019.

Gorkowski, K., Donahue, N. M., and Sullivan, R. C.: Emulsified and Liquid–Liquid Phase-Separated States of α-Pinene Secondary Organic Aerosol Determined Using Aerosol Optical Tweezers, Environmental Science & Technology, 51, 12154-12163, 10.1021/acs.est.7b03250, 2017.

Gorkowski, K., Donahue, N. M., and Sullivan, R. C.: Aerosol Optical Tweezers Constrain the Morphology Evolution of Liquid-Liquid Phase-Separated Atmospheric Particles, Chem, 6, 204-220, https://doi.org/10.1016/j.chempr.2019.10.018, 2020.

Heine, N., Arata, C., Goldstein, A. H., Houle, F. A., and Wilson, K. R.: Multiphase Mechanism for the Production of Sulfuric Acid from SO2 by Criegee Intermediates Formed During the Heterogeneous Reaction of Ozone with Squalene, The Journal of Physical Chemistry Letters, 9, 3504-3510, 10.1021/acs.jpclett.8b01171, 2018.

Huang, Q., Wei, H., Marr, L. C., and Vikesland, P. J.: Direct Quantification of the Effect of Ammonium on Aerosol Droplet pH, Environmental Science & Technology, 10.1021/acs.est.0c07394, 2020.

Huang, Y., Mahrt, F., Xu, S., Shiraiwa, M., Zuend, A., and Bertram, A. K.: Coexistence of three liquid phases in individual atmospheric aerosol particles, Proceedings of the National Academy of Sciences, 118, e2102512118, 10.1073/pnas.2102512118, 2021.

Huffman, J. A., Perring, A. E., Savage, N. J., Clot, B., Crouzy, B., Tummon, F., Shoshanim, O., Damit, B., Schneider, J., Sivaprakasam, V., Zawadowicz, M. A., Crawford, I., Gallagher, M., Topping, D., Doughty, D. C., Hill, S. C., and Pan, Y.: Real-time sensing of bioaerosols: Review and current perspectives, Aerosol Science and Technology, 54, 465-495, 10.1080/02786826.2019.1664724, 2020.

Ishizaka, S., Yamamoto, C., and Yamagishi, H.: Liquid–Liquid Phase Separation of Single Optically Levitated Water–Ionic Liquid Droplets in Air, The Journal of Physical Chemistry A, 125, 7716-7722, 10.1021/acs.jpca.1c06130, 2021.

Ivleva, N. P., McKeon, U., Niessner, R., and Pöschl, U.: Raman Microspectroscopic Analysis of Size-Resolved Atmospheric Aerosol Particle Samples Collected with an ELPI: Soot, Humic-Like Substances, and Inorganic Compounds, Aerosol Science and Technology, 41, 655-671, 10.1080/02786820701376391, 2007a.

Ivleva, N. P., Messerer, A., Yang, X., Niessner, R., and Pöschl, U.: Raman Microspectroscopic Analysis of Changes in the Chemical Structure and Reactivity of Soot in a Diesel Exhaust Aftertreatment Model System, Environmental Science & Technology, 41, 3702-3707, 10.1021/es0612448, 2007b.

Jacobs, M. I., Davies, J. F., Lee, L., Davis, R. D., Houle, F., and Wilson, K. R.: Exploring Chemistry in Microcompartments Using Guided Droplet Collisions in a Branched Quadrupole Trap Coupled to a Single Droplet, Paper Spray Mass Spectrometer, Analytical Chemistry, 89, 12511-12519, 10.1021/acs.analchem.7b03704, 2017.

Jarvis, R. M., Law, N., Shadi, I. T., O'Brien, P., Lloyd, J. R., and Goodacre, R.: Surface-Enhanced Raman Scattering from Intracellular and Extracellular Bacterial Locations, Analytical Chemistry, 80, 6741-6746, 10.1021/ac800838v, 2008.

Jones, R. R., Hooper, D. C., Zhang, L., Wolverson, D., and Valev, V. K.: Raman techniques: Fundamentals and frontiers, Nanoscale research letters, 14, 1-34, 2019.

Jones, S. H., Friederich, P., and Donaldson, D. J.: Photochemical Aging of Levitated Aqueous Brown Carbon Droplets, ACS Earth and Space Chemistry, 5, 749-754, 10.1021/acsearthspacechem.1c00005, 2021.

Kalume, A., Beresnev, L. A., Santarpia, J., and Pan, Y.-L.: Detection and characterization of chemical aerosol using laser-trapping single-particle Raman spectroscopy, Appl. Opt., 56, 6577-6582, 10.1364/AO.56.006577, 2017a.

Kalume, A., Zhu, E., Wang, C., Santarpia, J., and Pan, Y.-L.: Position-resolved Raman spectra from a laser-trapped single airborne chemical droplet, Opt. Lett., 42, 5113-5116, 10.1364/OL.42.005113, 2017b.

Kalume, A., Wang, C., Santarpia, J., and Pan, Y.-L.: Liquid–liquid phase separation and evaporation of a laser-trapped organic–organic airborne droplet using temporal spatial-resolved Raman spectroscopy, Physical Chemistry Chemical Physics, 20, 19151-19159, 10.1039/C8CP02372G, 2018.

Kampf, C. J., Liu, F., Reinmuth-Selzle, K., Berkemeier, T., Meusel, H., Shiraiwa, M., and Pöschl, U.: Protein Cross-Linking and Oligomerization through Dityrosine Formation upon Exposure to Ozone, Environmental Science & Technology, 49, 10859-10866, 10.1021/acs.est.5b02902, 2015.

Kang, E., Root, M. J., Toohey, D. W., and Brune, W. H.: Introducing the concept of Potential Aerosol Mass (PAM), Atmos. Chem. Phys., 7, 5727-5744, 10.5194/acp-7-5727-2007, 2007.

Keller, A., and Burtscher, H.: A continuous photo-oxidation flow reactor for a defined measurement of the SOA formation potential of wood burning emissions, Journal of aerosol science, 49, 9-20, 2012.

Kerminen, V.-M., Chen, X., Vakkari, V., Petäjä, T., Kulmala, M., and Bianchi, F.: Atmospheric new particle formation and growth: review of field observations, Environmental Research Letters, 13, 103003, 2018.

King, M. D., Thompson, K. C., and Ward, A. D.: Laser tweezers Raman study of optically trapped aerosol droplets of seawater and oleic acid reacting with ozone: implications for cloud-droplet properties, Journal of the American chemical society, 126, 16710-16711, 2004.

King, M. D., Thompson, K. C., Ward, A. D., Pfrang, C., and Hughes, B. R.: Oxidation of biogenic and water-soluble compounds in aqueous and organic aerosol droplets by ozone: a kinetic and product analysis approach using laser Raman tweezers, Faraday Discussions, 137, 173-192,

1244   10.1039/B702199B, 2008.

1245 Kirkby, J., Curtius, J., Almeida, J., Dunne, E., Duplissy, J., Ehrhart, S., Franchin, A., Gagné, S., Ickes,

1246   L., and Kürten, A.: Role of sulphuric acid, ammonia and galactic cosmic rays in atmospheric

1247   aerosol nucleation, Nature, 476, 429-433, 2011.

1248 Kline, N. J., and Treado, P. J.: Raman chemical imaging of breast tissue, Journal of Raman Spectroscopy,

1249   28, 119-124, 1997.

1250 Knopf, D., Koop, T., Luo, B., Weers, U., and Peter, T.: Homogeneous nucleation of NAD and NAT in

1251   liquid stratospheric aerosols: insufficient to explain denitrification, 2002.

1252 Knopf, D. A., Luo, B. P., Krieger, U. K., and Koop, T.: Thermodynamic Dissociation Constant of the

1253   Bisulfate Ion from Raman and Ion Interaction Modeling Studies of Aqueous Sulfuric Acid at

1254   Low Temperatures, The Journal of Physical Chemistry A, 107, 4322-4332, 10.1021/jp027775+,

1255   2003.

1256 Kohli, R. K., and Davies, J. F.: Measuring the Chemical Evolution of Levitated Particles: A Study on the

1257   Evaporation of Multicomponent Organic Aerosol, Analytical Chemistry, 93, 12472-12479,

1258   2021.

1259 Krieger, U. K., Marcolli, C., and Reid, J. P.: Exploring the complexity of aerosol particle properties and

1260   processes using single particle techniques, Chemical Society Reviews, 41, 6631-6662, 2012.

1261 Kunihisa, R., Iwata, A., Gen, M., Chan, C. K., and Matsuki, A.: Application of SERS on the chemical

1262   speciation of individual Aitken mode particles after condensational growth, Aerosol Science

1263   and Technology, 54, 826-836, 10.1080/02786826.2020.1730298, 2020.

1264 Kuwata, M., and Martin, S. T.: Phase of atmospheric secondary organic material affects its reactivity,

1265   Proc Natl Acad Sci U S A, 109, 17354-17359, 10.1073/pnas.1209071109, 2012.

1266 Kwamena, N. O. A., Buajarern, J., and Reid, J. P.: Equilibrium Morphology of Mixed

1267   Organic/Inorganic/Aqueous Aerosol Droplets: Investigating the Effect of Relative Humidity

1268   and Surfactants, The Journal of Physical Chemistry A, 114, 5787-5795, 10.1021/jp1003648,

1269   2010.

1270 Lam, H. K., Xu, R., Choczynski, J., Davies, J. F., Ham, D., Song, M., Zuend, A., Li, W., Tse, Y. L. S.,

1271   and Chan, M. N.: Effects of liquid–liquid phase separation and relative humidity on the

1272   heterogeneous OH oxidation of inorganic–organic aerosols: insights from methylglutaric acid

1273   and ammonium sulfate particles, Atmos. Chem. Phys., 21, 2053-2066, 10.5194/acp-21-2053-

1274   2021, 2021.

1275 Laskin, A., Laskin, J., and Nizkorodov, S. A.: Chemistry of atmospheric brown carbon, Chem Rev, 115,

1276   4335-4382, 10.1021/cr5006167, 2015.

1277 Laskina, O., Young, M. A., Kleiber, P. D., and Grassian, V. H.: Infrared extinction spectroscopy and

1278   micro-Raman spectroscopy of select components of mineral dust mixed with organic

1279   compounds, Journal of Geophysical Research: Atmospheres, 118, 6593-6606,

1280   https://doi.org/10.1002/jgrd.50494, 2013.

1281 Laskina, O., Morris, H. S., Grandquist, J. R., Qin, Z., Stone, E. A., Tivanski, A. V., and Grassian, V. H.:

1282   Size Matters in the Water Uptake and Hygroscopic Growth of Atmospherically Relevant

1283   Multicomponent Aerosol Particles, The Journal of Physical Chemistry A, 119, 4489-4497,

1284   10.1021/jp510268p, 2015.

1285 Laucks, M. L., Roll, G., Schweiger, G., and Davis, E. J.: PHYSICAL AND CHEMICAL (RAMAN)

1286   CHARACTERIZATION OF BIOAEROSOLS—POLLEN, Journal of Aerosol Science, 31,

1287   307-319, https://doi.org/10.1016/S0021-8502(99)00058-0, 2000.

Lee, A. K., Ling, T., and Chan, C. K.: Understanding hygroscopic growth and phase transformation of aerosols using single particle Raman spectroscopy in an electrodynamic balance, Faraday Discussions, 137, 245-263, 2008a.

Lee, A. K. Y., and Chan, C. K.: Single particle Raman spectroscopy for investigating atmospheric heterogeneous reactions of organic aerosols, Atmospheric Environment, 41, 4611-4621, https://doi.org/10.1016/j.atmosenv.2007.03.040, 2007a.

Lee, A. K. Y., and Chan, C. K.: Heterogeneous Reactions of Linoleic Acid and Linolenic Acid Particles with Ozone: Reaction Pathways and Changes in Particle Mass, Hygroscopicity, and Morphology, The Journal of Physical Chemistry A, 111, 6285-6295, 10.1021/jp071812l, 2007b.

Lee, A. K. Y., Li, Y. J., Lau, A. P. S., and Chan, C. K.: A Re-Evaluation on the Atmospheric Significance of Octanal Vapor Uptake by Acidic Particles: Roles of Particle Acidity and Gas-Phase Octanal Concentration, Aerosol Science and Technology, 42, 992-1000, 10.1080/02786820802382736, 2008b.

Lee, J. S., Ahn, Y., Kim, J., Kim, J., Nam, S. H., Yu, S.-C., Shin, H. H., Jung, T., Kim, E.-A., Suh, Y. D., Kim, H. W., and Park, H.-R.: Chemical analysis of air pollutant particulate matters based on surface enhanced Raman spectroscopy (SERS), SPIE Nanoscience + Engineering, SPIE, 2019.

Li, J. F., Huang, Y. F., Ding, Y., Yang, Z. L., Li, S. B., Zhou, X. S., Fan, F. R., Zhang, W., Zhou, Z. Y., Wu, D. Y., Ren, B., Wang, Z. L., and Tian, Z. Q.: Shell-isolated nanoparticle-enhanced Raman spectroscopy, Nature, 464, 392-395, 10.1038/nature08907, 2010.

Li, R., Palm, B. B., Ortega, A. M., Hlywiak, J., Hu, W., Peng, Z., Day, D. A., Knote, C., Brune, W. H., de Gouw, J. A., and Jimenez, J. L.: Modeling the Radical Chemistry in an Oxidation Flow Reactor: Radical Formation and Recycling, Sensitivities, and the OH Exposure Estimation Equation, The Journal of Physical Chemistry A, 119, 4418-4432, 10.1021/jp509534k, 2015.

Li, X., Gupta, D., Lee, J., Park, G., and Ro, C.-U.: Real-Time Investigation of Chemical Compositions and Hygroscopic Properties of Aerosols Generated from NaCl and Malonic Acid Mixture Solutions Using in Situ Raman Microspectrometry, Environmental Science & Technology, 51, 263-270, 10.1021/acs.est.6b04356, 2017.

Li, X., Wu, L., Lee, J.-S., and Ro, C.-U.: Hygroscopic behavior and chemical reactivity of aerosols generated from mixture solutions of low molecular weight dicarboxylic acids and NaCl, Physical Chemistry Chemical Physics, 23, 11052-11064, 2021.

Li, Y. J., Lee, A. K., Lau, A. P., and Chan, C. K.: Accretion reactions of octanal catalyzed by sulfuric acid: Product identification, reaction pathways, and atmospheric implications, Environmental science & technology, 42, 7138-7145, 2008.

Liang, Z., Zhang, R., Gen, M., Chu, Y., and Chan, C. K.: Nitrate Photolysis in Mixed Sucrose–Nitrate–Sulfate Particles at Different Relative Humidities, The Journal of Physical Chemistry A, 10.1021/acs.jpca.1c00669, 2021.

Ling, T. Y., and Chan, C. K.: Formation and Transformation of Metastable Double Salts from the Crystallization of Mixed Ammonium Nitrate and Ammonium Sulfate Particles, Environmental Science & Technology, 41, 8077-8083, 10.1021/es071419t, 2007.

Ling, T. Y., and Chan, C. K.: Partial crystallization and deliquescence of particles containing ammonium sulfate and dicarboxylic acids, Journal of Geophysical Research: Atmospheres, 113, https://doi.org/10.1029/2008JD009779, 2008.

Liu, T., Wang, X., Hu, Q., Deng, W., Zhang, Y., Ding, X., Fu, X., Bernard, F., Zhang, Z., Lü, S., He, Q., Bi, X., Chen, J., Sun, Y., Yu, J., Peng, P., Sheng, G., and Fu, J.: Formation of secondary aerosols

from gasoline vehicle exhaust when mixing with SO2, Atmos. Chem. Phys., 16, 675-689, 10.5194/acp-16-675-2016, 2016.

Liu, T., and Abbatt, J. P.: An experimental assessment of the importance of S (IV) oxidation by hypohalous acids in the marine atmosphere, Geophysical Research Letters, 47, e2019GL086465, 2020.

Liu, T., Clegg, S. L., and Abbatt, J. P.: Fast oxidation of sulfur dioxide by hydrogen peroxide in deliquesced aerosol particles, Proceedings of the National Academy of Sciences, 117, 1354-1359, 2020a.

Liu, T., and Abbatt, J. P. D.: Oxidation of sulfur dioxide by nitrogen dioxide accelerated at the interface of deliquesced aerosol particles, Nature Chemistry, 13, 1173-1177, 10.1038/s41557-021-00777-0, 2021.

Liu, T., Chan, A. W. H., and Abbatt, J. P. D.: Multiphase Oxidation of Sulfur Dioxide in Aerosol Particles: Implications for Sulfate Formation in Polluted Environments, Environmental Science & Technology, 55, 4227-4242, 10.1021/acs.est.0c06496, 2021.

Liu, X., Knauer, M., Ivleva, N. P., Niessner, R., and Haisch, C.: Synthesis of Core−Shell Surface-Enhanced Raman Tags for Bioimaging, Analytical Chemistry, 82, 441-446, 10.1021/ac902573p, 2010.

Liu, Y., Zhu, T., Zhao, D., and Zhang, Z.: Investigation of the hygroscopic properties of Ca (NO 3) 2 and internally mixed Ca (NO 3) 2/CaCO 3 particles by micro-Raman spectrometry, 2008.

Liu, Y., Zhou, H., Hu, Z., Yu, G., Yang, D., and Zhao, J.: Label and label-free based surface-enhanced Raman scattering for pathogen bacteria detection: A review, Biosensors and Bioelectronics, 94, 131-140, https://doi.org/10.1016/j.bios.2017.02.032, 2017.

Liu, Y., Wang, T., Fang, X., Deng, Y., Cheng, H., Bacha, A.-U.-R., Nabi, I., and Zhang, L.: Brown carbon: An underlying driving force for rapid atmospheric sulfate formation and haze event, Science of The Total Environment, 734, 139415, https://doi.org/10.1016/j.scitotenv.2020.139415, 2020b.

Lu, J. W., Isenor, M., Chasovskikh, E., Stapfer, D., and Signorell, R.: Low-temperature Bessel beam trap for single submicrometer aerosol particle studies, Review of Scientific Instruments, 85, 095107, 2014.

Ma, Q., Liu, C., Ma, J., Chu, B., and He, H.: A laboratory study on the hygroscopic behavior of H2C2O4-containing mixed particles, Atmospheric Environment, 200, 34-39, https://doi.org/10.1016/j.atmosenv.2018.11.056, 2019a.

Ma, Q., Zhong, C., Liu, C., Liu, J., Ma, J., Wu, L., and He, H.: A Comprehensive Study about the Hygroscopic Behavior of Mixtures of Oxalic Acid and Nitrate Salts: Implication for the Occurrence of Atmospheric Metal Oxalate Complex, ACS Earth and Space Chemistry, 3, 1216-1225, 10.1021/acsearthspacechem.9b00077, 2019b.

Ma, S., Chen, Z., Pang, S., and Zhang, Y.: Observations on hygroscopic growth and phase transitions of mixed 1, 2, 6-hexanetriol / (NH4)2SO4 particles: investigation of the liquid–liquid phase separation (LLPS) dynamic process and mechanism and secondary LLPS during the dehumidification, Atmos. Chem. Phys., 21, 9705-9717, 10.5194/acp-21-9705-2021, 2021.

Mabato, B. R. G., Gen, M., Chu, Y., and Chan, C. K.: Reactive Uptake of Glyoxal by Methylaminium-Containing Salts as a Function of Relative Humidity, ACS Earth and Space Chemistry, 3, 150-157, 10.1021/acsearthspacechem.8b00154, 2019.

Mael, L. E., Busse, H., and Grassian, V. H.: Measurements of Immersion Freezing and Heterogeneous Chemistry of Atmospherically Relevant Single Particles with Micro-Raman Spectroscopy,

Analytical Chemistry, 91, 11138-11145, 10.1021/acs.analchem.9b01819, 2019.

Mael, L. E., Busse, H. L., Peiker, G., and Grassian, V. H.: Low-Temperature Water Uptake of Individual Marine and Biologically Relevant Atmospheric Particles Using Micro-Raman Spectroscopy, The Journal of Physical Chemistry A, 125, 9691-9699, 10.1021/acs.jpca.1c08037, 2021.

Marcolli, C., and Krieger, U. K.: Relevance of particle morphology for atmospheric aerosol processing, Trends in Chemistry, 2, 1-3, 2020.

Marsh, A., Miles, R. E. H., Rovelli, G., Cowling, A. G., Nandy, L., Dutcher, C. S., and Reid, J. P.: Influence of organic compound functionality on aerosol hygroscopicity: dicarboxylic acids, alkyl-substituents, sugars and amino acids, Atmos. Chem. Phys., 17, 5583-5599, 10.5194/acp-17-5583-2017, 2017.

Marsh, A., Rovelli, G., Miles, R. E. H., and Reid, J. P.: Complexity of Measuring and Representing the Hygroscopicity of Mixed Component Aerosol, The Journal of Physical Chemistry A, 123, 1648-1660, 10.1021/acs.jpca.8b11623, 2019.

Mekic, M., Wang, Y., Loisel, G., Vione, D., and Gligorovski, S.: Ionic Strength Effect Alters the Heterogeneous Ozone Oxidation of Methoxyphenols in Going from Cloud Droplets to Aerosol Deliquescent Particles, Environmental Science & Technology, 54, 12898-12907, 10.1021/acs.est.0c03648, 2020.

Meresman, H., Wills, J. B., Summers, M., McGloin, D., and Reid, J. P.: Manipulation and characterisation of accumulation and coarse mode aerosol particles using a Bessel beam trap, Physical Chemistry Chemical Physics, 11, 11333-11339, 2009.

Mikhailov, E., Vlasenko, S., Martin, S. T., Koop, T., and Pöschl, U.: Amorphous and crystalline aerosol particles interacting with water vapor: conceptual framework and experimental evidence for restructuring, phase transitions and kinetic limitations, Atmos. Chem. Phys., 9, 9491-9522, 10.5194/acp-9-9491-2009, 2009.

Miles, R. E. H., Walker, J. S., Burnham, D. R., and Reid, J. P.: Retrieval of the complex refractive index of aerosol droplets from optical tweezers measurements, Physical Chemistry Chemical Physics, 14, 3037-3047, 10.1039/C2CP23999J, 2012.

Milsom, A., Squires, A. M., Boswell, J. A., Terrill, N. J., Ward, A. D., and Pfrang, C.: An organic crystalline state in ageing atmospheric aerosol proxies: spatially resolved structural changes in levitated fatty acid particles, Atmos. Chem. Phys., 21, 15003-15021, 10.5194/acp-21-15003-2021, 2021.

Mitchem, L., Buajarern, J., Hopkins, R. J., Ward, A. D., Gilham, R. J. J., Johnston, R. L., and Reid, J. P.: Spectroscopy of Growing and Evaporating Water Droplets: Exploring the Variation in Equilibrium Droplet Size with Relative Humidity, The Journal of Physical Chemistry A, 110, 8116-8125, 10.1021/jp061135f, 2006.

Mitchem, L., and Reid, J. P.: Optical manipulation and characterisation of aerosol particles using a single-beam gradient force optical trap, Chemical Society Reviews, 37, 756-769, 10.1039/B609713H, 2008.

Mosier-Boss, P. A.: Review on SERS of Bacteria, Biosensors, 7, 51, 2017.

Movasaghi, Z., Rehman, S., and Rehman, I. U.: Raman Spectroscopy of Biological Tissues, Applied Spectroscopy Reviews, 42, 493-541, 10.1080/05704920701551530, 2007.

Nadler, K. A., Kim, P., Huang, D.-L., Xiong, W., and Continetti, R. E.: Water diffusion measurements of single charged aerosols using H2O/D2O isotope exchange and Raman spectroscopy in an electrodynamic balance, Physical Chemistry Chemical Physics, 21, 15062-15071,

1420   10.1039/C8CP07052K, 2019.

1421   Nakajima, R., Miura, A., Abe, S., and Kitamura, N.: Optical Trapping–Polarized Raman
1422   Microspectroscopy of Single Ethanol Aerosol Microdroplets: Droplet Size Effects on Rotational
1423   Relaxation Time and Viscosity, Analytical Chemistry, 93, 5218-5224,
1424   10.1021/acs.analchem.0c05406, 2021.

1425   Nishikida, K., Nishio, E., and Hannah, R. W.: Selected applications of modern FT-IR techniques,
1426   Routledge, 2018.

1427   Offroy, M., Moreau, M., Sobanska, S., Milanfar, P., and Duponchel, L.: Pushing back the limits of Raman
1428   imaging by coupling super-resolution and chemometrics for aerosols characterization,
1429   Scientific Reports, 5, 12303, 10.1038/srep12303, 2015.

1430   Ofner, J., Deckert-Gaudig, T., Kamilli, K. A., Held, A., Lohninger, H., Deckert, V., and Lendl, B.: Tip-
1431   Enhanced Raman Spectroscopy of Atmospherically Relevant Aerosol Nanoparticles, Analytical
1432   Chemistry, 88, 9766-9772, 10.1021/acs.analchem.6b02760, 2016.

1433   Olson, N. E., Lei, Z., Craig, R. L., Zhang, Y., Chen, Y., Lambe, A. T., Zhang, Z., Gold, A., Surratt, J. D.,
1434   and Ault, A. P.: Reactive Uptake of Isoprene Epoxydiols Increases the Viscosity of the Core of
1435   Phase-Separated Aerosol Particles, ACS Earth and Space Chemistry, 3, 1402-1414,
1436   10.1021/acsearthspacechem.9b00138, 2019.

1437   Pajunoja, A., Hu, W., Leong, Y. J., Taylor, N. F., Miettinen, P., Palm, B. B., Mikkonen, S., Collins, D. R.,
1438   Jimenez, J. L., and Virtanen, A.: Phase state of ambient aerosol linked with water uptake and
1439   chemical aging in the southeastern US, Atmospheric Chemistry and Physics, 16, 11163-11176,
1440   2016.

1441   Pan, Y.-L., Hill, S. C., and Coleman, M.: Photophoretic trapping of absorbing particles in air and
1442   measurement of their single-particle Raman spectra, Opt. Express, 20, 5325-5334,
1443   10.1364/OE.20.005325, 2012.

1444   Parmentier, E. A., David, G., Arroyo, P. C., Bibawi, S., Esat, K., and Signorell, R.: Photochemistry of
1445   single optically trapped oleic acid droplets, Journal of Aerosol Science, 151, 105660,
1446   https://doi.org/10.1016/j.jaerosci.2020.105660, 2021.

1447   Parsons, M. T., Mak, J., Lipetz, S. R., and Bertram, A. K.: Deliquescence of malonic, succinic, glutaric,
1448   and adipic acid particles, Journal of Geophysical Research: Atmospheres, 109,
1449   https://doi.org/10.1029/2003JD004075, 2004.

1450   Peng, C., Chan, M. N., and Chan, C. K.: The Hygroscopic Properties of Dicarboxylic and Multifunctional
1451   Acids: Measurements and UNIFAC Predictions, Environmental Science & Technology, 35,
1452   4495-4501, 10.1021/es0107531, 2001.

1453   Peng, Z., and Jimenez, J. L.: Radical chemistry in oxidation flow reactors for atmospheric chemistry
1454   research, Chemical Society Reviews, 49, 2570-2616, 10.1039/C9CS00766K, 2020.

1455   Pöschl, U.: Atmospheric Aerosols: Composition, Transformation, Climate and Health Effects,
1456   Angewandte Chemie International Edition, 44, 7520-7540,
1457   https://doi.org/10.1002/anie.200501122, 2005.

1458   Power, R., Simpson, S., Reid, J., and Hudson, A.: The transition from liquid to solid-like behaviour in
1459   ultrahigh viscosity aerosol particles, Chemical Science, 4, 2597-2604, 2013.

1460   Price, C. L., Bain, A., Wallace, B. J., Preston, T. C., and Davies, J. F.: Simultaneous Retrieval of the Size
1461   and Refractive Index of Suspended Droplets in a Linear Quadrupole Electrodynamic Balance,
1462   The Journal of Physical Chemistry A, 124, 1811-1820, 10.1021/acs.jpca.9b10748, 2020.

1463   Qin, Y., Ye, J., Ohno, P., Zhai, J., Han, Y., Liu, P., Wang, J., Zaveri, R. A., and Martin, S. T.: Humidity

Dependence of the Condensational Growth of α-Pinene Secondary Organic Aerosol Particles, Environmental Science & Technology, 55, 14360-14369, 10.1021/acs.est.1c01738, 2021.

Qiu, J., Ishizuka, S., Tonokura, K., and Enami, S.: Interfacial vs Bulk Ozonolysis of Nerolidol, Environmental Science & Technology, 53, 5750-5757, 10.1021/acs.est.9b00364, 2019.

Qiu, J., Liang, Z., Tonokura, K., Colussi, A. J., and Enami, S.: Stability of Monoterpene-Derived α-Hydroxyalkyl-Hydroperoxides in Aqueous Organic Media: Relevance to the Fate of Hydroperoxides in Aerosol Particle Phases, Environmental Science & Technology, 54, 3890-3899, 10.1021/acs.est.9b07497, 2020.

Radić, N., and Prkić, A.: Historical remarks on the Henderson-Hasselbalch equation: its advantages and limitations and a novel approach for exact pH calculation in buffer region, Reviews in Analytical Chemistry, 31, 93-98, 2012.

Rafferty, A., and Preston, T. C.: Measuring the size and complex refractive index of an aqueous aerosol particle using electromagnetic heating and cavity-enhanced Raman scattering, Physical Chemistry Chemical Physics, 20, 17038-17047, 10.1039/C8CP02966K, 2018.

Redding, B., Hill, S. C., Alexson, D., Wang, C., and Pan, Y.-L.: Photophoretic trapping of airborne particles using ultraviolet illumination, Opt. Express, 23, 3630-3639, 10.1364/OE.23.003630, 2015a.

Redding, B., and Pan, Y.-L.: Optical trap for both transparent and absorbing particles in air using a single shaped laser beam, Opt. Lett., 40, 2798-2801, 10.1364/OL.40.002798, 2015.

Redding, B., Schwab, M. J., and Pan, Y.-l.: Raman spectroscopy of optically trapped single biological micro-particles, Sensors, 15, 19021-19046, 2015b.

Reid, J. P., and Mitchem, L.: LASER PROBING OF SINGLE-AEROSOL DROPLET DYNAMICS, Annual Review of Physical Chemistry, 57, 245-271, 10.1146/annurev.physchem.57.032905.104621, 2006.

Renbaum-Wolff, L., Song, M., Marcolli, C., Zhang, Y., Liu, P. F., Grayson, J. W., Geiger, F. M., Martin, S. T., and Bertram, A. K.: Observations and implications of liquid–liquid phase separation at high relative humidities in secondary organic material produced by α-pinene ozonolysis without inorganic salts, Atmospheric Chemistry and Physics, 16, 7969-7979, 2016.

Richards, D. S., Trobaugh, K. L., Hajek-Herrera, J., Price, C. L., Sheldon, C. S., Davies, J. F., and Davis, R. D.: Ion-molecule interactions enable unexpected phase transitions in organic-inorganic aerosol, Science Advances, 6, eabb5643, 10.1126/sciadv.abb5643, 2020.

Rindelaub, J. D., Craig, R. L., Nandy, L., Bondy, A. L., Dutcher, C. S., Shepson, P. B., and Ault, A. P.: Direct Measurement of pH in Individual Particles via Raman Microspectroscopy and Variation in Acidity with Relative Humidity, The Journal of Physical Chemistry A, 120, 911-917, 10.1021/acs.jpca.5b12699, 2016.

Rkiouak, L., Tang, M., Camp, J., McGregor, J., Watson, I., Cox, R., Kalberer, M., Ward, A., and Pope, F.: Optical trapping and Raman spectroscopy of solid particles, Physical Chemistry Chemical Physics, 16, 11426-11434, 2014.

Rodriguez, R. D., Sheremet, E., Deckert-Gaudig, T., Chaneac, C., Hietschold, M., Deckert, V., and Zahn, D. R. T.: Surface- and tip-enhanced Raman spectroscopy reveals spin-waves in iron oxide nanoparticles, Nanoscale, 7, 9545-9551, 10.1039/C5NR01277E, 2015.

Rosati, B., Paul, A., Iversen, E. M., Massling, A., and Bilde, M.: Reconciling atmospheric water uptake by hydrate forming salts, Environmental Science: Processes & Impacts, 22, 1759-1767, 2020.

Rovelli, G., Miles, R. E. H., Reid, J. P., and Clegg, S. L.: Accurate Measurements of Aerosol Hygroscopic

Growth over a Wide Range in Relative Humidity, The Journal of Physical Chemistry A, 120, 4376-4388, 10.1021/acs.jpca.6b04194, 2016.

Roy, P., Mael, L. E., Makhnenko, I., Martz, R., Grassian, V. H., and Dutcher, C. S.: Temperature-Dependent Phase Transitions of Aqueous Aerosol Droplet Systems in Microfluidic Traps, ACS Earth and Space Chemistry, 4, 1527-1539, 10.1021/acsearthspacechem.0c00114, 2020.

Rygula, A., Majzner, K., Marzec, K. M., Kaczor, A., Pilarczyk, M., and Baranska, M.: Raman spectroscopy of proteins: a review, Journal of Raman Spectroscopy, 44, 1061-1076, 2013.

Sahoo, S. K., Umapathy, S., and Parker, A. W.: Time-Resolved Resonance Raman Spectroscopy: Exploring Reactive Intermediates, Applied Spectroscopy, 65, 1087-1115, 2011.

Saniel, M. B. B., Lim, L. H. V., and Lamorena, R. B.: An Initial Study on the Feasibility of Using Rudimentary SERS in Quick Chemical Assessment of Ambient Aerosols, ChemistrySelect, 4, 14082-14090, https://doi.org/10.1002/slct.201903479, 2019.

Sauerwein, M., and Chan, C. K.: Heterogeneous uptake of ammonia and dimethylamine into sulfuric and oxalic acid particles, Atmospheric Chemistry & Physics, 17, 2017.

Schill, G. P., De Haan, D. O., and Tolbert, M. A.: Heterogeneous Ice Nucleation on Simulated Secondary Organic Aerosol, Environmental Science & Technology, 48, 1675-1682, 10.1021/es4046428, 2014.

Scolaro, S., Sobanska, S., Barbillat, J., Laureyns, J., Louis, F., Petitprez, D., and Brémard, C.: Confocal Raman imaging and atomic force microscopy of the surface reaction of NO2 and NaCl (100) under humidity, Journal of Raman Spectroscopy: An International Journal for Original Work in all Aspects of Raman Spectroscopy, Including Higher Order Processes, and also Brillouin and Rayleigh Scattering, 40, 157-163, 2009.

Seinfeld, J. H., and Pandis, S. N.: Atmospheric chemistry and physics: from air pollution to climate change, John Wiley & Sons, 2016.

Seng, S., Guo, F., Tobon, Y. A., Ishikawa, T., Moreau, M., Ishizaka, S., and Sobanska, S.: Deliquescence behavior of photo-irradiated single NaNO3 droplets, Atmospheric Environment, 183, 33-39, https://doi.org/10.1016/j.atmosenv.2018.04.007, 2018.

Sengupta, A., Laucks, M. L., Dildine, N., Drapala, E., and Davis, E. J.: Bioaerosol characterization by surface-enhanced Raman spectroscopy (SERS), Journal of Aerosol Science, 36, 651-664, https://doi.org/10.1016/j.jaerosci.2004.11.001, 2005.

Setschenow, J.: Über die Konstitution der Salzlösungen auf Grund ihres Verhaltens zu Kohlensäure, Zeitschrift für Physikalische Chemie, 4U, 117, https://doi.org/10.1515/zpch-1889-0409, 1889.

Singh, M., Mayya, Y. S., Gaware, J., and Thaokar, R. M.: Levitation dynamics of a collection of charged droplets in an electrodynamic balance, Journal of Applied Physics, 121, 054503, 10.1063/1.4974470, 2017.

Singh, M., Thaokar, R., Khan, A., and Mayya, Y. S.: Theoretical analysis of formation of many-drop arrays in a quadrupole electrodynamic balance, Physical Review E, 98, 032202, 10.1103/PhysRevE.98.032202, 2018.

Sivaprakasam, V., Hart, M. B., and Eversole, J. D.: Surface Enhanced Raman Spectroscopy of Individual Suspended Aerosol Particles, The Journal of Physical Chemistry C, 121, 22326-22334, 10.1021/acs.jpcc.7b05310, 2017.

Sivaprakasam, V., and Hart, M. B.: Surface-Enhanced Raman Spectroscopy for Environmental Monitoring of Aerosols, ACS Omega, 10.1021/acsomega.1c00207, 2021.

Smith, J., Kroll, J., Cappa, C., Che, D., Liu, C., Ahmed, M., Leone, S., Worsnop, D., and Wilson, K.: The

heterogeneous reaction of hydroxyl radicals with sub-micron squalane particles: a model system for understanding the oxidative aging of ambient aerosols, Atmospheric Chemistry and Physics, 9, 3209-3222, 2009.

Sobanska, S., Falgayrac, G., Laureyns, J., and Brémard, C.: Chemistry at level of individual aerosol particle using multivariate curve resolution of confocal Raman image, Spectrochimica Acta Part A: Molecular and Biomolecular Spectroscopy, 64, 1102-1109, https://doi.org/10.1016/j.saa.2005.11.038, 2006.

Sobanska, S., Falgayrac, G., Rimetz-Planchon, J., Perdrix, E., Brémard, C., and Barbillat, J.: Resolving the internal structure of individual atmospheric aerosol particle by the combination of Atomic Force Microscopy, ESEM–EDX, Raman and ToF–SIMS imaging, Microchemical Journal, 114, 89-98, https://doi.org/10.1016/j.microc.2013.12.007, 2014.

Sobanska, S., Dappe, V., Siepka, D., Moreau, M., Tobon, Y., and Stefaniak, E. A.: Automated Raman microspectrometry and Raman imaging for atmospheric particle, Euroanalysis 2015, Bordeaux, France, 2015-09, 2015.

Socrates, G.: Infrared and Raman characteristic group frequencies: tables and charts, John Wiley & Sons, 2004.

Song, M., Marcolli, C., Krieger, U., Zuend, A., and Peter, T.: Liquid-liquid phase separation in aerosol particles: Dependence on O: C, organic functionalities, and compositional complexity, Geophysical research letters, 39, 2012a.

Song, M., Marcolli, C., Krieger, U., Zuend, A., and Peter, T.: Liquid-liquid phase separation and morphology of internally mixed dicarboxylic acids/ammonium sulfate/water particles, Atmospheric Chemistry and Physics, 12, 2691-2712, 2012b.

Song, M., Marcolli, C., Krieger, U. K., Lienhard, D. M., and Peter, T.: Morphologies of mixed organic/inorganic/aqueous aerosol droplets, Faraday discussions, 165, 289-316, 2013.

Song, M., Ham, S., Andrews, R. J., You, Y., and Bertram, A. K.: Liquid–liquid phase separation in organic particles containing one and two organic species: importance of the average O: C, Atmospheric Chemistry and Physics, 18, 12075-12084, 2018.

Steer, B., Gorbunov, B., Price, M. C., and Podoleanu, A.: Raman spectroscopic identification of size-selected airborne particles for quantitative exposure assessment, Measurement Science and Technology, 27, 045801, 2016.

Stewart, D. J., Cai, C., Nayler, J., Preston, T. C., Reid, J. P., Krieger, U. K., Marcolli, C., and Zhang, Y. H.: Liquid–Liquid Phase Separation in Mixed Organic/Inorganic Single Aqueous Aerosol Droplets, The Journal of Physical Chemistry A, 119, 4177-4190, 10.1021/acs.jpca.5b01658, 2015.

Su, H., Cheng, Y., and Pöschl, U.: New Multiphase Chemical Processes Influencing Atmospheric Aerosols, Air Quality, and Climate in the Anthropocene, Accounts of Chemical Research, 53, 2034-2043, 10.1021/acs.accounts.0c00246, 2020.

Sullivan, R. C., Boyer-Chelmo, H., Gorkowski, K., and Beydoun, H.: Aerosol Optical Tweezers Elucidate the Chemistry, Acidity, Phase Separations, and Morphology of Atmospheric Microdroplets, Accounts of Chemical Research, 53, 2498-2509, 10.1021/acs.accounts.0c00407, 2020.

Sun, Z., Duan, F., He, K., Du, J., Yang, L., Li, H., Ma, T., and Yang, S.: Physicochemical analysis of individual atmospheric fine particles based on effective surface-enhanced Raman spectroscopy, Journal of Environmental Sciences, 75, 388-395, https://doi.org/10.1016/j.jes.2018.06.006,

2019a.

Sun, Z., Duan, F., He, K., Du, J., and Zhu, L.: Sulfate–nitrate–ammonium as double salts in PM2.5: Direct observations and implications for haze events, Science of The Total Environment, 647, 204-209, https://doi.org/10.1016/j.scitotenv.2018.07.107, 2019b.

Tahir, M. A., Zhang, X., Cheng, H., Xu, D., Feng, Y., Sui, G., Fu, H., Valev, V. K., Zhang, L., and Chen, J.: Klarite as a label-free SERS-based assay: a promising approach for atmospheric bioaerosol detection, Analyst, 145, 277-285, 10.1039/C9AN01715A, 2020.

Talari, A. C. S., Movasaghi, Z., Rehman, S., and Rehman, I. U.: Raman spectroscopy of biological tissues, Applied spectroscopy reviews, 50, 46-111, 2015.

Tang, M., Chan, C. K., Li, Y. J., Su, H., Ma, Q., Wu, Z., Zhang, G., Wang, Z., Ge, M., Hu, M., He, H., and Wang, X.: A review of experimental techniques for aerosol hygroscopicity studies, Atmos. Chem. Phys., 19, 12631-12686, 10.5194/acp-19-12631-2019, 2019.

Tang, M. J., Camp, J. C. J., Rkiouak, L., McGregor, J., Watson, I. M., Cox, R. A., Kalberer, M., Ward, A. D., and Pope, F. D.: Heterogeneous Interaction of SiO2 with N2O5: Aerosol Flow Tube and Single Particle Optical Levitation–Raman Spectroscopy Studies, The Journal of Physical Chemistry A, 118, 8817-8827, 10.1021/jp506753c, 2014.

Tirella, P. N., Craig, R. L., Tubbs, D. B., Olson, N. E., Lei, Z., and Ault, A. P.: Extending surface enhanced Raman spectroscopy (SERS) of atmospheric aerosol particles to the accumulation mode (150–800 nm), Environmental Science: Processes & Impacts, 20, 1570-1580, 10.1039/C8EM00276B, 2018.

Tobon, Y. A., Seng, S., Picone, L. A., Bava, Y. B., Juncal, L. C., Moreau, M., Romano, R. M., Barbillat, J., and Sobanska, S.: Photochemistry of single particles using acoustic levitation coupled with Raman microspectrometry, Journal of Raman Spectroscopy, 48, 1135-1137, https://doi.org/10.1002/jrs.5181, 2017.

Tobon, Y. A., El Hajj, D., Seng, S., Bengrad, F., Moreau, M., Visez, N., Chiapello, I., Crumeyrolle, S., and Choël, M.: Impact of the particle mixing state on the hygroscopicity of internally mixed sodium chloride–ammonium sulfate single droplets: a theoretical and experimental study, Physical Chemistry Chemical Physics, 23, 14391-14403, 2021.

Tolles, W. M., Nibler, J., McDonald, J., and Harvey, A.: A review of the theory and application of coherent anti-Stokes Raman spectroscopy (CARS), Applied Spectroscopy, 31, 253-271, 1977.

Treuel, L., Pederzani, S., and Zellner, R.: Deliquescence behaviour and crystallisation of ternary ammonium sulfate/dicarboxylic acid/water aerosols, Physical Chemistry Chemical Physics, 11, 7976-7984, 10.1039/B905007H, 2009.

Tripathi, A., Jabbour, R. E., Guicheteau, J. A., Christesen, S. D., Emge, D. K., Fountain, A. W., Bottiger, J. R., Emmons, E. D., and Snyder, A. P.: Bioaerosol Analysis with Raman Chemical Imaging Microspectroscopy, Analytical Chemistry, 81, 6981-6990, 10.1021/ac901074c, 2009.

Tsai, J.-H. M., Harrison, J. G., Martin, J. C., Hamilton, T. P., van der Woerd, M., Jablonsky, M. J., and Beckman, J. S.: Role of Conformation of Peroxynitrite Anion (ONOO-) with Its Stability and Toxicity, Journal of the American Chemical Society, 116, 4115-4116, 10.1021/ja00088a072, 1994.

Uraoka, M., Maegawa, K., and Ishizaka, S.: Raman Spectroscopy of Single Light-Absorbing Carbonaceous Particles Levitated in Air Using an Annular Laser Beam, Analytical Chemistry, 89, 12866-12871, 10.1021/acs.analchem.7b03455, 2017.

Vejpongsa, I., Suvachittanont, S., Klinklan, N., Thongyen, T., Veres, M., and Szymanski, W. W.:

Deliberation between PM1 and PM2.5 as air quality indicators based on comprehensive characterization of urban aerosols in Bangkok, Thailand, Particuology, 35, 1-9, https://doi.org/10.1016/j.partic.2017.05.001, 2017.

Wang, C., Pan, Y.-L., Hill, S. C., and Redding, B.: Photophoretic trapping-Raman spectroscopy for single pollens and fungal spores trapped in air, Journal of Quantitative Spectroscopy and Radiative Transfer, 153, 4-12, 2015a.

Wang, M., Zheng, N., Zhao, D., Shang, J., and Zhu, T.: Using Micro-Raman Spectroscopy to Investigate Chemical Composition, Mixing States, and Heterogeneous Reactions of Individual Atmospheric Particles, Environmental Science & Technology, 55, 10243-10254, 10.1021/acs.est.1c01242, 2021a.

Wang, W., Lei, T., Zuend, A., Su, H., Cheng, Y., Shi, Y., Ge, M., and Liu, M.: Effect of mixing structure on the water uptake of mixtures of ammonium sulfate and phthalic acid particles, Atmospheric Chemistry and Physics, 21, 2179-2190, 2021b.

Wang, X., Jing, B., Tan, F., Ma, J., Zhang, Y., and Ge, M.: Hygroscopic behavior and chemical composition evolution of internally mixed aerosols composed of oxalic acid and ammonium sulfate, Atmos. Chem. Phys., 17, 12797-12812, 10.5194/acp-17-12797-2017, 2017.

Wang, Y., Ma, J.-B., Zhou, Q., Pang, S.-F., and Zhang, Y.-H.: Hygroscopicity of Mixed Glycerol/Mg(NO3)2/Water Droplets Affected by the Interaction between Magnesium Ions and Glycerol Molecules, The Journal of Physical Chemistry B, 119, 5558-5566, 10.1021/acs.jpcb.5b00458, 2015b.

Wei, H., Vejerano, E. P., Leng, W., Huang, Q., Willner, M. R., Marr, L. C., and Vikesland, P. J.: Aerosol microdroplets exhibit a stable pH gradient, Proceedings of the National Academy of Sciences, 115, 7272-7277, 10.1073/pnas.1720488115, 2018.

Wheeler, M. J., Mason, R. H., Steunenberg, K., Wagstaff, M., Chou, C., and Bertram, A. K.: Immersion Freezing of Supermicron Mineral Dust Particles: Freezing Results, Testing Different Schemes for Describing Ice Nucleation, and Ice Nucleation Active Site Densities, The Journal of Physical Chemistry A, 119, 4358-4372, 10.1021/jp507875q, 2015.

Willis, M. D., Rovelli, G., and Wilson, K. R.: Combining Mass Spectrometry of Picoliter Samples with a Multicompartment Electrodynamic Trap for Probing the Chemistry of Droplet Arrays, Analytical Chemistry, 92, 11943-11952, 10.1021/acs.analchem.0c02343, 2020.

Wise, M. E., Baustian, K. J., and Tolbert, M. A.: Internally mixed sulfate and organic particles as potential ice nuclei in the tropical tropopause region, Proceedings of the National Academy of Sciences, 107, 6693-6698, 2010.

Wise, M. E., Baustian, K. J., Koop, T., Freedman, M. A., Jensen, E. J., and Tolbert, M. A.: Depositional ice nucleation onto crystalline hydrated NaCl particles: a new mechanism for ice formation in the troposphere, Atmospheric Chemistry and Physics, 12, 1121-1134, 2012.

Wu, F.-M., Wang, X.-W., Jing, B., Zhang, Y.-H., and Ge, M.-F.: Liquid-liquid phase separation in internally mixed magnesium sulfate/glutaric acid particles, Atmospheric Environment, 178, 286-292, https://doi.org/10.1016/j.atmosenv.2018.02.012, 2018a.

Wu, H. B., Chan, M. N., and Chan, C. K.: FTIR Characterization of Polymorphic Transformation of Ammonium Nitrate, Aerosol Science and Technology, 41, 581-588, 10.1080/02786820701272038, 2007.

Wu, H. B., and Chan, C. K.: Effects of potassium nitrate on the solid phase transitions of ammonium nitrate particles, Atmospheric Environment, 42, 313-322, 2008.

Wu, L., Becote, C., Sobanska, S., Flaud, P. M., Perraudin, E., Villenave, E., Song, Y. C., and Ro, C. U.: Hygroscopic behavior of aerosols generated from solutions of 3-methyl-1,2,3-butanetricarboxylic acid, its sodium salts, and its mixtures with NaCl, Atmos. Chem. Phys., 20, 14103-14122, 10.5194/acp-20-14103-2020, 2020.

Wu, Z., Wang, Y., Tan, T., Zhu, Y., Li, M., Shang, D., Wang, H., Lu, K., Guo, S., Zeng, L., and Zhang, Y.: Aerosol Liquid Water Driven by Anthropogenic Inorganic Salts: Implying Its Key Role in Haze Formation over the North China Plain, Environmental Science & Technology Letters, 5, 160-166, 10.1021/acs.estlett.8b00021, 2018b.

Xu, G., Cheng, H., Jones, R., Feng, Y., Gong, K., Li, K., Fang, X., Tahir, M. A., Valev, V. K., and Zhang, L.: Surface-Enhanced Raman Spectroscopy Facilitates the Detection of Microplastics <1 μm in the Environment, Environmental Science & Technology, 54, 15594-15603, 10.1021/acs.est.0c02317, 2020a.

Xu, R., Ge, Y., Kwong, K. C., Poon, H. Y., Wilson, K. R., Yu, J. Z., and Chan, M. N.: Inorganic Sulfur Species Formed upon Heterogeneous OH Oxidation of Organosulfates: A Case Study of Methyl Sulfate, ACS Earth and Space Chemistry, 4, 2041-2049, 10.1021/acsearthspacechem.0c00209, 2020b.

Ye, J., Abbatt, J. P. D., and Chan, A. W. H.: Novel pathway of SO2 oxidation in the atmosphere: reactions with monoterpene ozonolysis intermediates and secondary organic aerosol, Atmos. Chem. Phys., 18, 5549-5565, 10.5194/acp-18-5549-2018, 2018.

Yeung, M. C., and Chan, C. K.: Water Content and Phase Transitions in Particles of Inorganic and Organic Species and their Mixtures Using Micro-Raman Spectroscopy, Aerosol Science and Technology, 44, 269-280, 10.1080/02786820903583786, 2010.

Yeung, M. C., Ling, T. Y., and Chan, C. K.: Effects of the Polymorphic Transformation of Glutaric Acid Particles on Their Deliquescence and Hygroscopic Properties, The Journal of Physical Chemistry A, 114, 898-903, 10.1021/jp908250v, 2010.

You, Y., Renbaum-Wolff, L., Carreras-Sospedra, M., Hanna, S. J., Hiranuma, N., Kamal, S., Smith, M. L., Zhang, X., Weber, R. J., Shilling, J. E., Dabdub, D., Martin, S. T., and Bertram, A. K.: Images reveal that atmospheric particles can undergo liquid–liquid phase separations, Proceedings of the National Academy of Sciences, 109, 13188, 10.1073/pnas.1206414109, 2012.

Yu, J.-Y., Zhang, Y., Tan, S.-H., Liu, Y., and Zhang, Y.-H.: Observation on the Ion Association Equilibria in NaNO3 Droplets Using Micro-Raman Spectroscopy, The Journal of Physical Chemistry B, 116, 12581-12589, 10.1021/jp306367v, 2012.

Yu, T., Zhao, D., Song, X., and Zhu, T.: NO2-initiated multiphase oxidation of SO2 by O2 on CaCO3 particles, Atmos. Chem. Phys, 18, 6679-6689, 2018.

Zangmeister, C. D., and Pemberton, J. E.: Raman Spectroscopy of the Reaction of Sodium Chloride with Nitric Acid: Sodium Nitrate Growth and Effect of Water Exposure, The Journal of Physical Chemistry A, 105, 3788-3795, 10.1021/jp003374n, 2001.

Zardini, A. A., Sjogren, S., Marcolli, C., Krieger, U. K., Gysel, M., Weingartner, E., Baltensperger, U., and Peter, T.: A combined particle trap/HTDMA hygroscopicity study of mixed inorganic/organic aerosol particles, Atmos. Chem. Phys., 8, 5589-5601, 10.5194/acp-8-5589-2008, 2008.

Zhang, C., Ma, N., Fan, F., Yang, Y., Größ, J., Yan, J., Bu, L., Wang, Y., and Wiedensohler, A.: Hygroscopic growth of aerosol particles consisted of oxalic acid and its internal mixture with ammonium sulfate for the relative humidity ranging from 80% to 99.5%, Atmospheric

1728   Environment, 252, 118318, 2021a.

1729   Zhang, R., Wang, G., Guo, S., Zamora, M. L., Ying, Q., Lin, Y., Wang, W., Hu, M., and Wang, Y.:

1730   Formation of urban fine particulate matter, Chemical reviews, 115, 3803-3855, 2015.

1731   Zhang, R., Gen, M., Huang, D., Li, Y., and Chan, C. K.: Enhanced Sulfate Production by Nitrate

1732   Photolysis in the Presence of Halide Ions in Atmospheric Particles, Environmental Science &

1733   Technology, 54, 3831-3839, 10.1021/acs.est.9b06445, 2020a.

1734   Zhang, R., Gen, M., Fu, T.-M., and Chan, C. K.: Production of Formate via Oxidation of Glyoxal

1735   Promoted by Particulate Nitrate Photolysis, Environmental Science & Technology,

1736   10.1021/acs.est.0c08199, 2021b.

1737   Zhang, Y., Bao, F., Li, M., Xia, H., Huang, D., Chen, C., and Zhao, J.: Photoinduced Uptake and

1738   Oxidation of SO2 on Beijing Urban PM2.5, Environmental Science & Technology, 54, 14868-

1739   14876, 10.1021/acs.est.0c01532, 2020b.

1740   Zhang, Y.-H., and Chan, C. K.: Study of Contact Ion Pairs of Supersaturated Magnesium Sulfate

1741   Solutions Using Raman Scattering of Levitated Single Droplets, The Journal of Physical

1742   Chemistry A, 104, 9191-9196, 10.1021/jp0013659, 2000.

1743   Zhang, Y.-H., and Chan, C. K.: Observations of Water Monomers in Supersaturated NaClO4, LiClO4,

1744   and Mg(ClO4)2 Droplets Using Raman Spectroscopy, The Journal of Physical Chemistry A,

1745   107, 5956-5962, 10.1021/jp0271256, 2003.

1746   Zhang, Y.-H., Choi, M. Y., and Chan, C. K.: Relating Hygroscopic Properties of Magnesium Nitrate to

1747   the Formation of Contact Ion Pairs, The Journal of Physical Chemistry A, 108, 1712-1718,

1748   10.1021/jp036524d, 2004.

1749   Zhao, D., Song, X., Zhu, T., Zhang, Z., Liu, Y., and Shang, J.: Multiphase oxidation of SO2 by NO2 on

1750   CaCO3 particles, Atmospheric Chemistry and Physics, 18, 2481-2493, 10.5194/acp-18-2481-

1751   2018, 2018.

1752   Zheng, G., Su, H., Wang, S., Andreae, M. O., Pöschl, U., and Cheng, Y.: Multiphase buffer theory

1753   explains contrasts in atmospheric aerosol acidity, Science, 369, 1374-1377, 2020a.

1754   Zheng, H., Song, S., Sarwar, G., Gen, M., Wang, S., Ding, D., Chang, X., Zhang, S., Xing, J., and Sun,

1755   Y.: Contribution of Particulate Nitrate Photolysis to Heterogeneous Sulfate Formation for

1756   Winter Haze in China, Environmental Science & Technology Letters, 7, 632-638, 2020b.

1757   Zheng, L., Kulkarni, P., Birch, M. E., Ashley, K., and Wei, S.: Analysis of Crystalline Silica Aerosol

1758   Using Portable Raman Spectrometry: Feasibility of Near Real-Time Measurement, Analytical

1759   Chemistry, 90, 6229-6239, 10.1021/acs.analchem.8b00830, 2018.

1760   Zhou, H., Yang, D., Ivleva, N. P., Mircescu, N. E., Niessner, R., and Haisch, C.: SERS Detection of

1761   Bacteria in Water by in Situ Coating with Ag Nanoparticles, Analytical Chemistry, 86, 1525-

1762   1533, 10.1021/ac402935p, 2014a.

1763   Zhou, H., Yang, D., Ivleva, N. P., Mircescu, N. E., Schubert, S., Niessner, R., Wieser, A., and Haisch, C.:

1764   Label-Free in Situ Discrimination of Live and Dead Bacteria by Surface-Enhanced Raman

1765   Scattering, Analytical Chemistry, 87, 6553-6561, 10.1021/acs.analchem.5b01271, 2015.

1766   Zhou, Q., Pang, S.-F., Wang, Y., Ma, J.-B., and Zhang, Y.-H.: Confocal Raman studies of the evolution

1767   of the physical state of mixed phthalic acid/ammonium sulfate aerosol droplets and the effect

1768   of substrates, The Journal of Physical Chemistry B, 118, 6198-6205, 2014b.

1769   Zhu, F., Zhou, H., Wang, X., Zhou, Y., Liu, H., Fang, C., and Fang, Y.: Raman spectroscopy and ab initio

1770   quantum chemical calculations of ion association behavior in calcium nitrate solution, Journal

1771   of Raman Spectroscopy, 49, 852-861, https://doi.org/10.1002/jrs.5349, 2018.

1772 Zobrist, B., Soonsin, V., Luo, B. P., Krieger, U. K., Marcolli, C., Peter, T., and Koop, T.: Ultra-slow water

1773   diffusion in aqueous sucrose glasses, Physical Chemistry Chemical Physics, 13, 3514-3526,

1774   2011.

1775
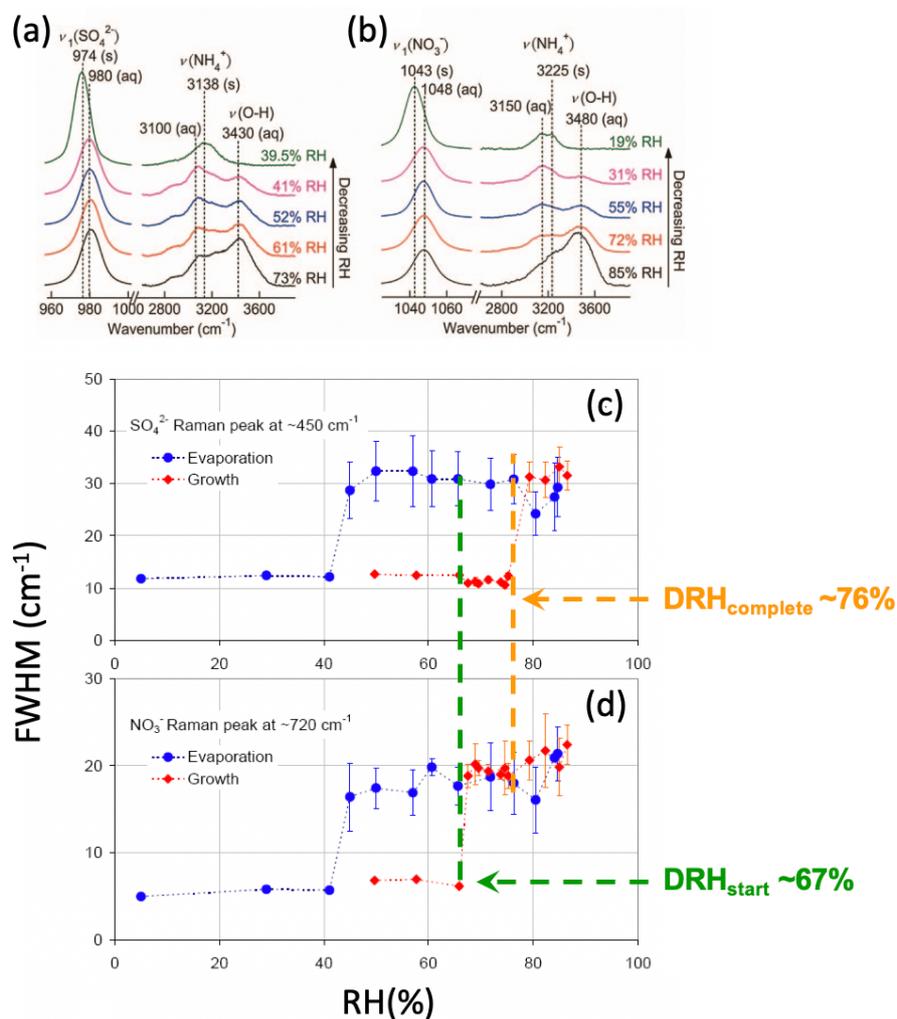
1776

Figure 1. Raman spectra of a single (a) AS and (b) AN particle upon evaporation (Yeung and Chan,

2010). FWHM of (c) SO_4^{2-} peak and (d) NO_3^- peak during the evaporation-growth cycle of a mixed AS-
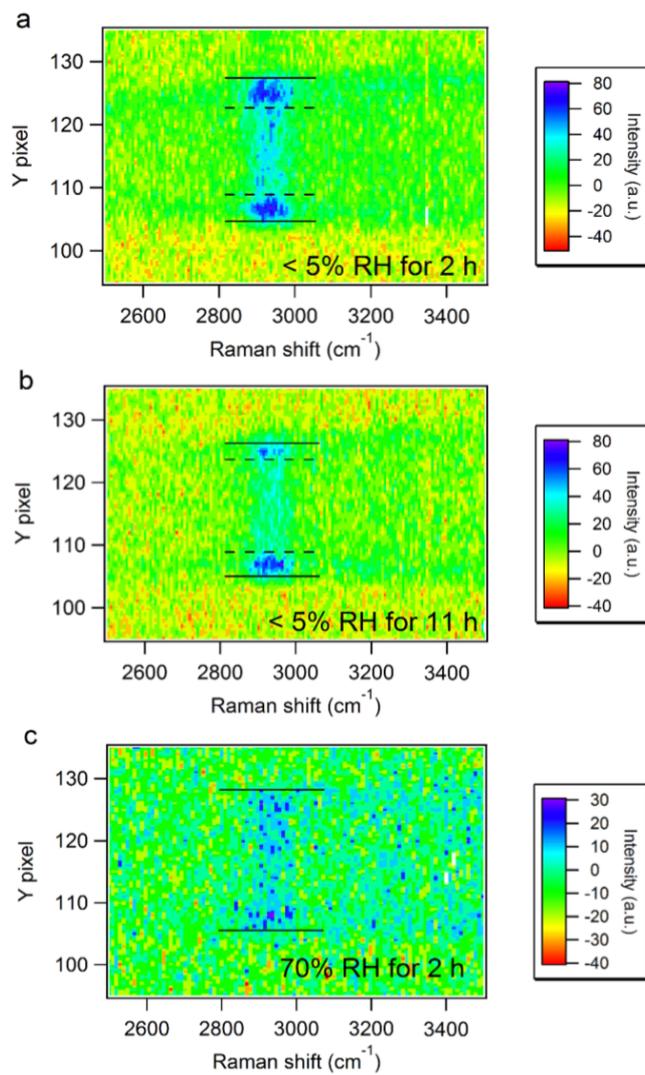
AN particle.

1780
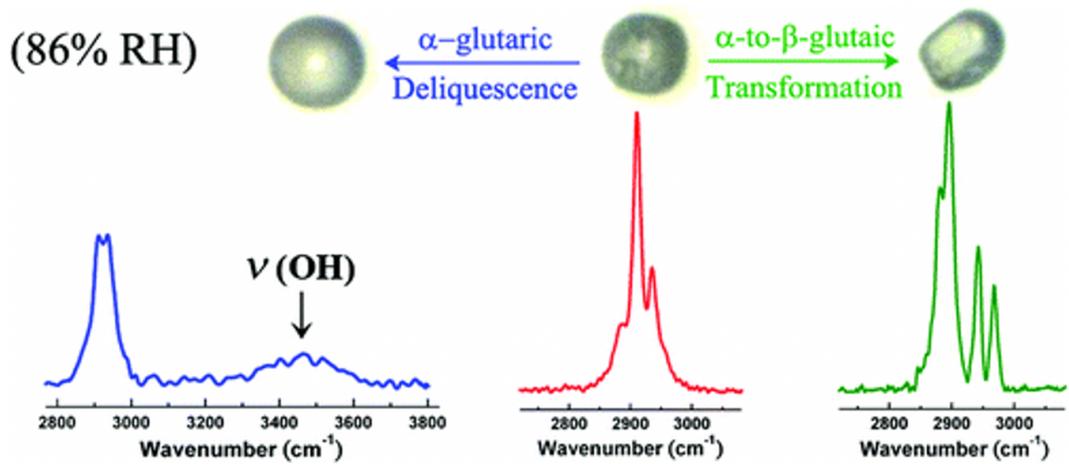
1781

Figure 2. Raman spectra of deliquescent α-glutaric acid, crystalline α-glutaric acid and β-glutaric acid

(Ling and Chan, 2007).


1785

Figure 3. Spatially resolved Raman intensities of AS – sucrose (molar fraction of sucrose in total solute

1787   (F_{SU}) = 0.5)) particles equilibrated (a) at < 5% RH for 2 hours and (b) for 11 h and (c) at 70% RH for 2

1788   hours. C-H peaks at ~2900 cm^{-1} represent sucrose. Solid lines indicate the particle's upper and lower

1789   edges. The outer regions between the dashed and solid lines are sucrose-rich in (a)-(b) (Chu and Chan,

1790   2017a).

1791
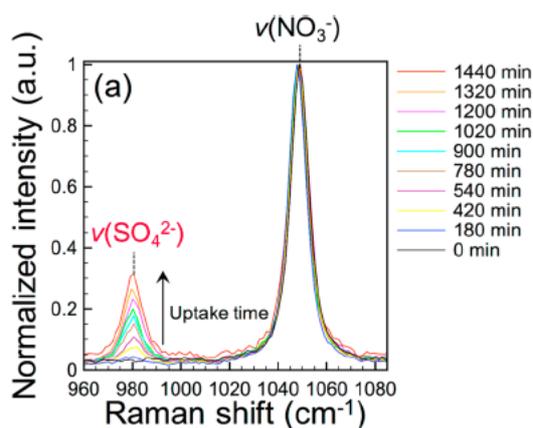
1792

1793   **Figure 4.** Sulfate formation during the photolysis of AN particles in the presence of SO_2 at 80% RH (Gen

1794   et al., 2019b).

1795
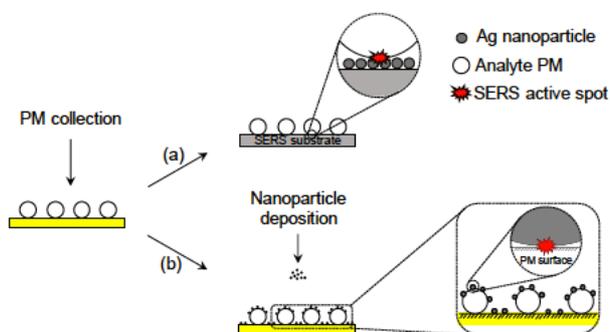
1796

1797   **Figure 5.** Schematic illustration of (a) a conventional SERS substrate approach and (b) the ES-SERS

1798   approach (Gen and Chan, 2017).

1799

1800   Appendix A. Major Raman peaks of atmospheric relevant species

Species		Raman shift (cm^{-1})	Ref.
Water	O-H	~3300 (monomers)	(Carey and
		~3600 (hydrogen-bonded)	Korenowski,
			1998)

Inorganic	NH_4^+	~1413; ~1660; ~3100	(Chu and Chan, 2017a;Sauerwein and Chan, 2017)
	SO_4^{2-}	~450; ~618; ~980	(Ling and Chan, 2007;Chu and Chan, 2017a)
	HSO_4^-	~1053	(Rindelaub et al., 2016;Craig et al., 2017;Craig et al., 2018)
	NO_3^-	~717; ~1046; ~1413	(Tobon et al., 2017;Gen et al., 2019b)
	HNO_3	~1306	(Rindelaub et al., 2016)
	NO_2^-	~815; ~1278; ~ 1330	(Tobon et al., 2017)
	$ONOO^-$	~980	(Tsai et al., 1994;Tobon et al., 2017)
	CO_3^{2-}	~1067	(Rindelaub et al., 2016)
	HCO_3^-	~1019	(Rindelaub et al., 2016)
Soot	D	~1367	(Ivleva et al., 2007b;Gen and Chan, 2017)
	G	~1585	(Ivleva et al., 2007b;Gen and

					Chan, 2017)
Mineral dust	SiO$_2$	Si-O-Si	~390; ~490; ~795; ~972; ~1460		(Laskina et al., 2013;Rkiouak et al., 2014)
		O-Si-O	~356		
		Si-O	~465		
	α-Al$_2$O$_3$	Al-O-Al	~420; ~585; ~796;		(Rkiouak et al., 2014)
		Al-OH	~976		
	Kaolinite	Si-O	~397		(Laskina et al., 2013)
		Si-O-Al	~516		
		O-H	~914; 3624; 3656; 3668; 3698		
	TiO$_2$	Ti-O	~484; ~680;	Amorphous	(Rkiouak et al., 2014;Tang et al., 2014)
			~153; ~639;	Anatase	
		O-O	~250; ~317;	Amorphous	
	CaCO$_3$	CO$_3^{2-}$	~713; ~1087		(Laskina et al., 2013;Yu et al., 2018;Zhao et al., 2018)
Organic	C-H		~1400; 2700-3000		(Chu and Chan, 2017a;Gen et al., 2018b)
	C-O		~1470		(Laskina et al., 2013)
	C=O		~1700		(Yeung and Chan, 2010;Yeung et al., 2010;Bondy et al., 2018)
	O-H		~1700; 3200-3400		(Yeung and Chan, 2010;Zhou et al., 2014b)

	C-N-C	~890	(Chu and Chan, 2017a)
	O-C-O (ring)	~770	(Gen et al., 2018b)
	ring	~950	(Gen et al., 2018b)
	O-O	~850	(Lee and Chan, 2007b, a)
	C=C	~1600	(Lee and Chan, 2007b;Chu et al., 2019)
	C=C-C=C	~1640&1655 (double peaks)	(Lee and Chan, 2007b;Chu et al., 2019)
	C=C-C=O	~1690	(Lee and Chan, 2007b;Chu et al., 2019)
	RO-SO$_3$	~846	(Bondy et al., 2018)
	S-O (-SO$_3$ group)	1065	(Bondy et al., 2018)

1801